Synthetic STARR-seq reveals how DNA shape and sequence modulate transcriptional output and noise.

Stefanie Schöne[1], Melissa Bothe[1], Edda Einfeldt[1], Marina Borschiwer[1], Philipp Benner[1], Martin Vingron[1], Morgane Thomas-Chollier[2], Sebastiaan H. Meijsing[1]

[1] *Max Planck Institute for Molecular Genetics, Ihnestraße 63-67, 14195 Berlin, Germany.*

[2] *Institut de biologie de l'Ecole normale supérieure (IBENS), Ecole normale supérieure, CNRS, INSERM, PSL Université Paris, 75005 Paris, France.*

Contact information:

Sebastiaan H. Meijsing

Max Planck Institute for Molecular Genetics,

Ihnestrasse 63-73

14195, Berlin, Germany

Tel: +49-30-84131176

Email: meijsing@molgen.mpg.de

Abstract

The binding of transcription factors to short recognition sequences plays a pivotal role in controlling the expression of genes. The sequence and shape characteristics of binding sites influence DNA binding specificity and have also been implicated in modulating the activity of transcription factors downstream of binding. To quantitatively assess the transcriptional activity of dozens of thousands of designed synthetic sites in parallel, we developed a synthetic version of STARR-seq (synSTARR-seq). We used the approach to systematically analyze how variations in the recognition sequence of the glucocorticoid receptor (GR) affect transcriptional regulation. Our approach resulted in the identification of a novel highly active functional GR binding sequence and revealed that sequence variation both within and flanking GR's core binding site can modulate GR activity without apparent changes in DNA binding affinity. Notably, we found that the sequence composition of variants with similar activity profiles was highly diverse. In contrast, groups of variants with similar activity profiles showed distinct DNA shape characteristics indicating that DNA shape may be a better predictor of activity than DNA sequence. Finally, using single cell experiments with individual enhancer variants, we obtained clues indicating that the architecture of the response element can independently tune expression mean and cell-to cell variability in gene expression (noise). Together, our studies establish synSTARR as a powerful method to systematically study how DNA sequence and shape modulate transcriptional output and noise.

Keywords

Enhancers, transcriptional regulation, glucocorticoid receptor, transcriptional noise, DNA shape

Introduction

The interplay between transcription factors (TFs) and genomically encoded *cis*-regulatory elements plays a key role in specifying where and when genes are expressed. In addition, the architecture of *cis*-regulatory elements influences the expression level of individual genes. For example, transcriptional output can be tuned by varying the number of TF binding sites, either for a given TF or for distinct TFs, present at an enhancer [1, 2]. Moreover, differences in its DNA-binding sites can modulate the magnitude of transcriptional activation, as exemplified by the glucocorticoid receptor (GR), a hormone-activated TF [3-5]. The sequence differences can reside within the 15 base pair (bp) core GR binding sequence (GBS) consisting of two imperfect 6 bp palindromic half-sites separated by a 3 bp spacer. Moreover, sequences directly flanking the core also modulate GR activity [3]. However, these sequence-induced changes in activity cannot be explained by affinity [3]. Instead, the flanking nucleotides induce structural changes in both DNA and the DNA binding domain of GR, arguing for their role in tuning GR activity [3].

Notably, the expression level of a gene is typically measured for populations of cells and thus masks that expression levels can vary considerably between individual cells of an isogenic population [6-9]. This variability in the expression level of a gene, called expression noise, results in phenotypic diversity, which can play a role in organismal responses to environmental changes (so called bet-hedging) and in cell fate decisions during development. Expression noise can be explained by the stochastic nature of the individual

steps that decode the information encoded in the genome. For example, transcription occurs in bursts [7, 10-12], which can induce variability in gene expression due to differences in burst frequency and in the number of transcripts generated per burst (burst size) [13]. Noise levels are gene-specific, which can be explained in part by differences in the sequence composition of *cis*-regulatory elements [11, 14-16]. For instance, the sequence composition of promoters influences expression variability with high burst size and noise for promoters containing a TATA box [15, 17]. In addition, chromatin and the presence or absence of nucleosome-disfavoring sequences have been linked to transcriptional noise [16-19]. Finally, noise levels can also be tuned by the number and by the affinity of TF binding sites [11, 16].

Many fundamental insights regarding the role of sequence in tuning transcriptional output and noise have come from reporter studies [20, 21]. A key advantage of reporters is that they can provide quantitative information in a controlled setting where everything is kept identical except for the sequence of the region of interest. Until recently, a limitation of reporter studies was that sequence variants had to be tested one at a time. However, the recent development of several parallelized reporter assays allows the simultaneous assessment of many sequence variants [21]. One of these parallelized methods is STARR-seq (Self-Transcribing Active Regulatory Region sequencing) [22]. In this assay, candidate sequences are placed downstream of a minimal promoter, such that active enhancers drive their own expression and high-throughput sequencing reveals both the sequence identity and quantitative information regarding the activity of each sequence variant. The STARR-seq method has been used to assay enhancer activity genome-wide [22, 23], to study regions of interest isolated either by Chromatin Immunoprecipitation (ChIP) or a capture-based approach [24, 25], and to study the effect of hormones on enhancer activity [25, 26].

Here, we adapted the STARR-seq method to systematically study how sequence variation both within the 15 bp GBS and in the region directly flanking it modulate GR activity. Specifically, we generated STARR-seq libraries using designed synthetic oligos (synSTARR-seq) with randomized nucleotides flanking the core GBS to show that the flanks modulate transcriptional output by almost an order of magnitude. When grouping sequences based on their ability to either enhance or blunt GBS activity, we found that each group contained a broad spectrum of highly diverse sequences, but striking similarities in their DNA shape characteristics. Using the same approach, we also assayed the effect of sequence variation within the core GBS. Finally, using single cell experiments with individual enhancer variants, we study how the sequence composition of the response element influences expression mean and noise. Together, our studies establish synSTARR-seq as a powerful method to study how DNA sequence and shape modulate transcriptional output and noise.

Results

Measuring the activity of thousands of GR binding sequence variants in parallel using the synSTARR-seq approach

To test if we could use the STARR-seq reporter [22] to study how sequence variation of the GR binding site influences GR activity, we first tested if a single GBS is sufficient to facilitate GR-dependent transcriptional activation of the reporter. Therefore, we constructed STARR reporters containing either a single GBS as candidate enhancer, a randomized sequence or as positive control a larger GBS-containing sequence derived from

a GR-bound region close to the GR target gene *FKBP5* (Fig. 1A). The resulting reporters were transfected into U2OS cells stably expressing GR (U2OS-GR) [27] and their response to treatment with dexamethasone (dex), a synthetic glucocorticoid hormone, was measured. As expected, no marked hormone-dependent induction was observed for the reporter with the randomized sequence. This was true both at the level of RNA (Fig. 1B) and at the level of the GFP reporter protein (Fig. S1A). In contrast, we observed a robust hormone-dependent activation both at the level of RNA and GFP protein for reporters with either a single GBS or with the larger genomic *FKBP5* fragment (Fig. 1B, S1A), showing that a single GBS is sufficient for GR-dependent activation of the STARR-seq reporter.

Our previous work has shown that the sequence directly flanking GBSs can modulate DNA shape and GR activity [3]. For a parallelized and thorough analysis of sequence variants flanking a GBS, we generated STARR-seq libraries for two GBS variants, we previously named Cgt and Sgk, that showed a strong influence of flanking nucleotides on activity [3]. Specifically, we generated libraries using designed synthetic sequences (synSTARR-seq) containing a GBS with five consecutive randomized nucleotides directly flanking the imperfect half site (Fig. 1A, S2A). Next, we transfected the GBS flank libraries into U2OS-GR cells to determine the activity of each of the 1024 flank variants present in the library. We performed three biological replicates for each condition and found that the results were highly reproducible ($r \geq 0.91$ for vehicle treated cells, $r \geq 0.98$ for dex treated cells; Fig. 1C, S1B-E). Notably, we retain duplicate reads in our analysis, which is essential to get quantitative information for individual sequence variants of the library. To calculate the activity for each flank variant, we used DESeq2 [28] to compare the RNA-seq read number between dex- and vehicle (ethanol) treated cells (Fig 1A). This resulted in the identification of 189 flank variants with significantly higher activity (enhancing flanks), 125 flank variants

144 with significantly lower activity (blunting flanks) and 710 flank variants that did not induce
145 significant changes in activity (neutral flanks). To test the accuracy of the synSTARR-seq
146 data, we cloned 5 flank variants from each activity group (enhancing, blunting and neutral)
147 and assayed the activity of each variant individually by qPCR. Consistent with what we
148 observed for the synSTARR library, the activity of blunting flanks was significantly lower
149 than for the neutral flanks whereas the activity of the enhancing flanks was significantly
150 higher (Fig. 1D). Notably, all flank variants tested were activated upon dex treatment
151 ranging from 2.1 to 15.3 fold (627% higher) depending on the sequence of the flank.
152 Together, our results show that the synSTARR-seq assay produces reproducible and
153 quantitative information and can be used for a high-throughput analysis of the effect of the
154 flanking sequence on GBS activity.
155
156 **SynSTARR-seq to assay the effect of flanking nucleotides**
157 To assess how the sequence composition of the flanking region influences GBS
158 activity, we ranked the flank variants by their activity and used a color chart representation
159 to plot the sequence at each position for the Cgt (Fig. 2A) and Sgk GBS (Fig. S2A),
160 respectively. In addition, we generated consensus sequence motifs for the significantly
161 enhancing and blunting variants (Fig. 2B, S2B). Notably, these consensus sequence motifs
162 treat each sequence equally and do not take the quantitative information regarding the
163 activity of each sequence into account. To take advantage of the quantitative information
164 provided by the synSTARR-seq assay, we used *k*pLogo [29], which uses the fold change as
165 weight for each sequence variant, and statistically evaluates the enrichment/depletion of
166 specific nucleotides at each position. The resulting probability logo can be interpreted as an
167 activity logo that visualizes for each position which nucleotides are associated with either

higher (letters above the coordinates) or lower (below the coordinates) GBS activity (Fig. 2C, S2C). The activity logo, consensus motifs and color chart highlight several sequence features for enhancing and blunting flank variants. For example, high activity is associated with a T at position 8 for both the Cgt and Sgk GBS, which matches what we found previously when we studied the activity of endogenous GR-bound regions [3]. In addition, the most active flank variants preferentially have an A at position 9 followed by a C at position 10 (Fig. 2A, S2A). To validate that this "TAC" signature results in high activity, we shuffled the sequence to either TCA or CAT and found that this indeed resulted in markedly lower activity (Fig. 2D). For blunting flank variants, we observed a preference for an A at position 8 and a bias against having a C at position 10 (Fig. 2A,C, S2A,C). However, altogether we find that the consensus motifs for enhancing and blunting flanks only have low information content and that a broad spectrum of distinct sequences can enhance or blunt the activity of the adjacent GBS (Fig. 2B, S2B).

Our previous work [3] indicates that DNA shape can influence GR activity downstream of binding. Consistent with this notion, we measured similar Kd values for flanks variants from the different activity classes (Fig. 2E). These findings are also in agreement with published work showing that the nucleotides directly flanking GBSs have little effect on GR affinity [30]. To examine if the flank effects might be explained by differences in DNA shape, we calculated the predicted minor groove width [31] for enhancing and blunting flank variants (Fig. 3A, S2D). Consistent with a role for DNA shape in modulating GR activity, we found shape characteristics that differ between enhancing and blunting flanks. For blunting flanks of the Cgt GBS, we observed a wider minor groove at position 6, and to a lesser degree at position 7 when compared to enhancing flanks (Fig. 3A, S3A). In addition, blunting flanks for the Cgt GBS have a narrower minor groove than

enhancing flanks for positions 8-12 (Fig. 3A, S3A), a region with several non-specific minor groove contacts with the C-terminal end of the DNA binding domain of GR [5]. For the Sgk GBS library, we find similar shape characteristics associated with blunting flanks with a wider minor groove at position 6 and a more narrow minor groove for positions 8-12 (Fig. S2D, S3B). DNA-shape- based hierarchical clustering recapitulates these characteristics in cluster 4, containing many more blunting flanks than any of the other clusters, for both the Cgt and Sgk GBS flank libraries (Fig. 3B,C, S2E,G). Of note, the consensus motifs for cluster 4 and for the other shape clusters have only low information content (Fig. 3D, S2F) indicating that distinct sequences can give rise to similar shape characteristics with shared effects on the activity of the adjacent GBS.

Together, these synSTARR-seq experiments uncover how sequence variation in the flanking region of the GBS influences activity and point at a role for DNA shape in modulating GBS activity.

SynSTARR-seq to assay the effect of variation within the core GBS

We next generated an additional synSTARR-seq library to study the effect of variation within the 15bp core sequence. This library contains a fixed GBS half site followed by eight consecutive randomized nucleotides (Fig. 4A). The library, containing over 65.000 variants, was transfected into U2OS-GR cells and the read count for each variant was determined both in the presence and absence of hormone treatment. Compared to the flank library, we observed a lower correlation between experiments, especially for variants with a low read count, which were removed before further analysis (Fig. S5). Next, we analyzed data from three biological replicates to determine the activity of variants in the library (Fig. 4B). To validate the measured activities, we cloned 4 sequences that repress, 4 that show a

weak activation (log2 fold change <2) and 8 strongly activating GBS variants. Consistent with the results from our screen, the three groups showed distinct levels of activity (Fig 4B,C). However, for the group of repressed GBS variants we did not recapitulate the observed repression in our screen (Fig 4C), indicating that these variants might behave differently in isolation or alternatively, that the repression might be a consequence of issues with data normalization. Notably, a lack of GR-dependent transcriptional repression was also reported in another study using the STARR-seq approach to study the regulatory activity of GR-bound genomic regions [25] indicating that GR might not be able to repress transcription in the STARR-seq context.

Given that the observed repression was not reproducible, we concentrated our analysis on 1696 sequences that facilitated significant GR-dependent transcriptional activation. Consistent with activation, we found that the consensus motif for activating sequence variants recapitulates the known GR consensus sequence with the second half site 3-bp downstream of the fixed first half site of our library (Fig. 4D). Accordingly, the GBS motif weight, which serves as a proxy for DNA binding affinity, is higher for activating sequences when compared to sequences that did not respond to hormone treatment (Fig. 4G). However, the score for the top 10% most active sequences was not higher than for all active variants (Fig. 4G), arguing that higher affinity does not drive the high levels of activation. As expected and consistent with the GR consensus motif, the color chart (Fig. 4D) and activity logo (Fig. 4E) highlight a strong preference for a G at position 3 and accordingly GBS activity is significantly lower for variants with a nucleotide other than G at this position (Fig. S7A). The activity logo also highlights that a G at position 2 is associated with lower activity (Fig. 4 E,F).

Previous studies have shown that the sequence of the spacer can modulate GBS activity [4, 5]. Therefore, we compared the activity of all 16 spacer variants in our library that match the GBS consensus for the second half site at the key positions 3, 4 and 6 (Fig. S6A). In line with a role for the spacer in modulating transcriptional output, we find significant differences between the spacer variants (Fig. S6B). For example, the activity for variants with an AC spacer is significantly higher than for most other spacer variants (Fig S6B) whereas the activity for GT variants is significantly lower ($p.adj < 0.01$) than either AA, AC or TC variants (Fig S6B).

Unexpectedly, the activity logo and top of the color chart indicated a high activity for variants with a C at position 2 (Fig. 4D,E), instead of a T usually observed in the GR consensus motif and from *in vitro* experiments studying the effect of DNA sequence on GR DNA binding affinity [30]. A careful examination of the sequence composition of the most active variants also revealed a preference for TC at the preceding positions within the spacer (Fig. 4E, 5A). To test if the high activity for sequences with a C at position 2 depends on the nucleotide composition of the preceding nucleotides, we changed them to GG and found that this resulted in a marked reduction in GR-dependent activation (Fig 5B, S8A). In addition, we compared the activity between variants with a T or a C at position 2. The activity was higher for the C variant when preceded by TC. However, when we changed the preceding nucleotides to GG the activation was stronger for the T than the C variant (Fig 5B, S8A). These experiments indicated that the high activity for the C variant depends on the preceding nucleotides.

Interestingly, the most active variants resemble the sequence composition of the "combi" motif we identified previously [32]. The combi motif contains only a single GR half site followed by TTCC and we found evidence that GR binds this sequence as a monomer in

conjunction with a partnering protein [32]. In contrast to the combi motif, the most active variants from our screen (named "combi2") also contain a recognizable second half site. To gain insight into the mode of GR binding at the combi2 motif, we examined published ChIP-exo data [32]. ChIP-exo is an assay that combines ChIP with a subsequent exonuclease step [33] which results in a base-pair resolution picture of GR binding. The ChIP-exo signal takes the form of sequence-specific peak patterns (footprint profiles), detectable on both strands with the program ExoProfiler [32]. We applied ExoProfiler to scan GR-bound regions with the combi2 motif (Fig. 5D,E, solid lines). As control, we analyzed the footprint profile for the canonical GR consensus motif (Fig. 5D; JASPAR MA0113.2) and recovered peak pairs on the forward and reverse flanks that demarcate the protection provided by each of the monomers of the GR dimer (Fig. 5E, shaded area). The signal for the first half site is essentially the same and a similar pattern is also observed for the second half site, indicating that GR binds as a dimer on regions bearing the combi2 motif, however with additional signal (highlighted with black arrows in Fig. 5E). In addition, we compared the footprint profile between the original combi (Fig. 5D; [32]) and the combi2 motif (Fig. 5F). Again, the position and shape of the peaks are compatible for the first half site but the ChIPexo signal for the second half site looks markedly different. The aforementioned additional signal for the combi2 motif aligns with the position of the second peak pair of the combi motif (Fig. 5F), indicating that the footprint profile for the combi2 motif appears to be a composite of the signal for homodimeric GR binding at canonical GBSs and the signal for monomeric GR binding together with another protein. Our previous work suggests that this partnering protein on combi motif might be Tead or ETS2. The ChIP-exo profile thus points to three alternative binding configurations on combi2: homodimeric GR, monomeric GR binding with Tead/ETS2 or the simultaneous binding of homodimeric GR complex

287 together with Tead/ETS2. Structural modeling suggests that this third mode is possible
288 given the absence of obvious sterical clashes that would prevent this mode of binding (Fig.
289 5G).

290 To assess if DNA shape could play a role in modulating GBS activity, we calculated
291 the predicted minor groove width for all 1696 significantly activated sequences ranked by
292 activity (Fig S7B). Comparison of the top 20% most active and bottom 20% least active
293 sequence variants highlighted two regions with significant differences. First, consistent
294 with our findings for the flank library, we find that a wider minor groove at positions 6 and
295 7 correlates with weaker activity (Fig. S7B,C). Second, we find that a narrower minor groove
296 in the spacer (position -1 and 0) correlates with weaker activity (Fig. S7B,C). As we
297 observed for the flank variants, the different activity classes do not show a distinct
298 sequence signature (Fig. S7B) again arguing that DNA shape might modulate GBS activity.

299 Together, the findings for our half site library suggest a role for both DNA shape and
300 sequence in tuning the activity of GBS variants. Moreover, our screen uncovered a novel
301 high-activity functional GR binding sequence variant.

302

303 **SynSTARR to assay the effect of enhancer sequence composition on noise.**

304 Thus far, we analyzed the effect of sequence composition on transcriptional output
305 by analyzing mean expression levels for populations of cells. To test if sequence variation in
306 the enhancer influences cell-to-cell variability in gene expression (noise), we measured GFP
307 levels for individual STARR constructs in single cells (Fig. 6A,B). Cells were transfected with
308 individual constructs along with an mCherry expression construct to remove extrinsic
309 noise, for example caused by differences in transfection efficiency. We first analyzed
310 sequence variants containing a single GBS (single GBS group) including known GBSs, two

311 variants matching the combi2 sequence motif and the Cgt GBS with an enhancing flank
312 variant. Consistent with previous findings [5], we found that GBS variants from the single
313 GBS group induced different mean levels of GFP expression. For example, the mean GFP
314 level upon dex treatment was lower for the pal GBS than for the Cgt variant (Fig. 6C, orange
315 and red squares). In line with findings by others [16], we observed that transcriptional
316 noise scales with mean expression with lower noise for variants with higher mean
317 expression (Fig. 6C). Next, we assayed two additional groups of sequences with distinct
318 binding sites architectures that both result in more robust GR-dependent activation when
319 compared to single GBS variants (Fig. 6A). The first group contained three instead of one
320 GBS copy (triple GBS group) whereas the second group (composite group) contains a GBS
321 flanked by a sequence motif for either AP1, ETS1 or SP1, three sequence motifs that can act
322 synergistically with GR [34, 35]. As expected, the mean GFP expression was higher for each
323 member of both the triple GBS and the composite group when compared to the single GBS
324 group (Fig 6A,C). Interestingly, the increase in mean expression we found for the groups of
325 triple GBS and composite enhancers was not accompanied by a decrease in expression
326 noise (Fig. 6C). The high noise to mean expression ratio was especially striking for several
327 triple GBS variants (3xPal, 3xCgt, 3xSgk and 3x Fkbp5-2) but observed in general for each
328 member of the groups of triple and composite enhancers when compared to the single GBS
329 group. Furthermore, enhancer variants with similar mean expression levels (*e.g.* 3xSgk and
330 Ets1+FKBP5-2) can have vastly different noise levels indicating that binding sites
331 architecture can independently tune both mean expression and cell-to-cell variability in
332 gene expression with noisier expression for enhancers with multiple GBSs.
333
334

Discussion:

In this study, we developed a modified version of the STARR-seq method where we used designed synthetic oligonucleotides to assay how sequence variation within and around the GBS influence GBS activity. This facilitated the thorough and parallelized assessment of 1024 flank variants on GBS activity in a highly reproducible and quantitative fashion (Fig. 1, S1). Similarly, we assessed over 65.000 variants to study how variations in one of the half sites and the spacer influence GBS activity. A key advantage of using designed sequences over the analysis of genomic regions is that variants can be compared in a context where everything is identical except for the sequence of the GR binding site. Notably, the sequence of the binding site is just one of several signals that are integrated at genomic response elements to modulate GR-dependent transcriptional responses. The synSTARR-seq approach can readily be adopted to study how combinations of signals are integrated. For example, principles of combinatorial regulation can be studied using designed sequences for which the GBS is flanked by binding sites for other TFs. Similarly, the assay can be used to investigate the cross-talk between GBS sequence, ligand chemistry, type of core promoter and GR splice isoforms.

Importantly, our findings for the synthetic STARR-seq assay are consistent with GR-dependent regulation of endogenous target genes. Specifically, the nucleotide directly flanking the GBS is preferentially a T for both enhancing flanks in our synSTARR-seq experiments and for the motif we previously found for genomic GR binding sites associated with genes that show the most robust response to GR activation [3]. Moreover, we uncovered a novel functional GR binding sequence variant with high activity, which we called combi2. Consistent with the high activity of the combi2 motif observed in the synSTARR assay, genes with nearby GR-bound peaks matching the combi2 motif were, on

359 average, slightly more activated by GR than genes with peaks matching the consensus motif
360 (Fig. 5C). Other sequence preferences we uncovered for flanks that enhance GBS activity
361 include an A followed by a C at positions 9 and 10 respectively (Fig. 2A,C; S2A,C). One
362 possible explanation for the increased activity is that this sequence generates an additional
363 GR half site or a binding site for another TF. However, the ChIP-exo profile for GBSs flanked
364 by nAC looked essentially the same as the profile for the canonical GBS (Fig. S4E), arguing
365 against the binding of an additional factor. Alternatively, the flanking nAC could influence
366 GR's DNA binding affinity. However, a comprehensive analysis of the effect of sequence
367 variation within and in the regions flanking GR binding sites showed that the flanks
368 essentially do not influence the binding affinity of GR [30]. Accordingly, we found similar Kd
369 values for the AC flank when compared to variants with lower activity (Fig. 2E) indicating
370 that the change in activity is not driven by affinity. Together, the synSTARR-seq approach
371 uncovered how sequence variation modulates GR activity, which confirmed previous
372 findings based on a small number of sequences but also provided new insights into
373 mechanisms that modulate GR-dependent regulation of endogenous target genes.

374 We were surprised to find that the consensus motifs for enhancing and blunting
375 flanks displayed low information content indicating that a broad spectrum of distinct
376 sequences can enhance or blunt the activity of the adjacent GBS (Fig. 2; Fig. S2). However,
377 when looking at DNA shape we found specific shape characteristics for each group (Fig. 3A).
378 This indicates that distinct sequences can induce similar DNA shape characteristics with
379 analogous effects on GBS activity. This finding was corroborated by our analysis of the
380 spacer, which is not directly contacted by GR, yet influences GR activity. Also here we found
381 distinct spacer shape characteristics for the most and least active GBS variants, without a
382 clear sequence signature for each group (Fig. S7B). Furthermore, we trained a model to

distinguish between high and low activity GBSs based on either DNA sequence or on predicted minor groove width information. Assessment of the accuracy of the models using ROC curves showed that a single shape parameter, minor groove width, can be used to distinguish quite accurately between blunting and enhancing flanks (Fig S9A) and also between the top and bottom 20% active GBS variants (Fig. S9B). Together, our findings which are based on a systematic analysis of many sequence variants are consistent with previous studies based on a small number of binding sites, showing that GR activity can be modulated by DNA shape [3, 4]. Notably, although the role of DNA shape in modulating the affinity of TFs for DNA has been well documented [36-38], we find that DNA shape modulates GR activity without apparent changes in DNA binding affinity (Fig. 2E, [30]). This is consistent with a model where DNA shape acts as an allosteric ligand which induces structural changes in associated TFs which in turn changes the composition and regulatory activity of the complexes formed at the response element [5, 39-41]. Another, not mutually exclusive explanation for flank-dependent modulation of transcriptional output is that flank variants serve as binding sites for other TFs that act additively or synergistically with GR. Further support for the importance of DNA shape comes from the analysis of the conservation of non-coding regions of the genome. This analysis uncovered greater conservation at the level of DNA shape than on the basis of nucleotide sequence indicating that DNA structure may be a better predictor of function than DNA sequence [42]. Accordingly, incorporation of DNA shape characteristics improves *in vivo* prediction of TF binding binding sites [43] and, based on our findings, could also improve the prediction of TF binding site activity.

We also explored if GFP protein expression levels of individual cells can be used to study how enhancer architecture influences cell-to-cell variability in gene expression. A

similar approach was used to study how sequence variation of the promoter influences transcriptional noise in yeast [16]. Notably, the only difference between the reporters we assayed is their enhancer sequence, which is downstream of the ORF for the GFP protein. For sequences with related enhancer architectures, we observed transcriptional noise scales with mean expression, such that higher expression levels are associated with lower noise (Fig. 6C). This is consistent with a two-state promoter model where increases in mean expression are driven by an upsurge in transcription burst frequency [44]. Similarly, the estrogen receptor, a hormone receptor closely related to GR, modulates transcription by changing the frequency of transcriptional bursting [12]. When we compare distinct enhancer architectures, we find that expression mean and noise can be uncoupled. Specifically, the noise to mean expression ratio is higher for response elements harboring multiple TF binding sites, indicating that the increase in expression might be accompanied by an increase in the number of transcripts produced during each burst. This finding is consistent with studies in yeast showing that increasing the number of binding sites for GCN4 results in increased expression with relatively high noise levels [16]. Notably, both multiple binding sites for GR and a combination of a GR binding site and a binding site for another TF result in an increased noise to mean expression ratio (Fig. 6). Our results are consistent with a model in which the architecture of the enhancer influences transcriptional burst size and frequency. However, more sophisticated single-cell studies of nascent transcripts are needed for a detailed understanding of the role of enhancer architecture given that our studies are based on the measurement of steady state fluctuations in protein levels. For example, in our experimental approach we cannot rule out that other mechanisms, including differences in RNA stability and translation rates, could contribute to the cell-to-cell variability in expression observed. Nonetheless, our findings argue that

differences in enhancer architecture might contribute to gene-specific tuning of expression mean to noise ratios of GR target genes.

Conclusions

Taken together, we present synSTARR, an approach to measure how designed binding site variants influence transcriptional output and noise. The systematic analysis of sequence variants presented here resulted in the identification of a novel functional GR binding sequence and provides evidence for an important role of DNA shape in tuning GR activity without apparent changes in DNA binding affinity. Our simple approach using designed sequences can be applied to other TFs and can be used to systematically unravel how the interplay between sequence and other signaling inputs at response elements modulate transcriptional output.

Materials and Methods

Experimental:

Plasmids.

STARR reporter constructs were generated by digesting the human STARR-seq vector [22] with SalI-HF and AgeI-HF and subsequent insertion of fragments of interest by in-Fusion HD cloning (TaKaRa). All inserts had the following sequence composition: 5'-**TAGAGCATGCACCGG**ACACTCTTTCCCTACACGACGCTCT----*INSERT*----AGATCGGAAGAGCACACGTCTGAACTCCAGTCAC**TCGACGAATTCGGCC**-3'. Sequence homologous to the STARR reporter construct in bold; Sequence for p5 and p7 adaptors

454 underlined. The exact sequence of the insert for each construct used in this study is listed in
455 table S1.
456
457 **Cell lines, transient transfections and luciferase assays.**
458 U2OS cells stably transfected with rat GRα (U2OS-GR18) [27] were grown in DMEM
459 supplemented with 5% FBS. Transient transfections were done essentially as described [5]
460 using either lipofectamine and plus reagents (Invitrogen) or using kit V for nucleofections
461 (Lonza).
462
463 **Synthetic STARR-seq**
464 Library design and generation: To generate GBS variant libraries, oligos containing
465 degenerate nucleotides (N) at defined positions were ordered from IDT as "DNA Ultramer
466 oligonucleotide" (sequence listed below). The oligonucleotides were made double stranded
467 using Phusion polymerase (NEB; 98°C for 35 sec, 72°C for 5 min) using the revPrimer
468 (GGCCGAATTCGTCGAGTGAC). The resulting double stranded inserts (25ng) were
469 recombined with 100ng linearized (SalI-HF and AgeI-HF) STARR-seq vector [22] by in-
470 Fusion cloning in 5 parallel reactions. After pooling the reactions, the DNA was cleaned up
471 using AMPure XP beads (Beckman Coulter), transformed into MegaX DH10B cells
472 (Invitrogen) and plasmid DNA was isolated using a Plasmid Plus Maxi kit (Qiagen). STARR-
473 seq: For STARR-seq experiments, 5 million U2OS-GR18 cells were transfected with 5 μg
474 library-DNA by nucleofection using kit V (Lonza). The next day, cells were treated for 4 h
475 with 1 μM dexamethasone or with 0.1% ethanol as vehicle control. Reverse transcription
476 and amplification of cDNA for subsequence Illumina 50bp paired-end sequencing were
477 done as described [22].

Cgt flank library DNA Ultramer oligonucleotide:

TAGAGCATGCACCGGACACTCTTTCCCTACACGACGCTCTTCCGATCTCAGCGCAAGAACAtttTGTACGNNNNNCTAG

ATCGGAAGAGCACACGTCTGAACTCCAGTCACTCGACGAATTCGGCC

Sgk flank library DNA Ultramer oligonucleotide:

TAGAGCATGCACCGGACACTCTTTCCCTACACGACGCTCTTCCGATCTCAGCGCAAGAACAtttTGTCCGNNNNNCTAG

ATCGGAAGAGCACACGTCTGAACTCCAGTCACTCGACGAATTCGGCC

GBS half site library DNA Ultramer oligonucleotide:

TAGAGCATGCACCGGACACTCTTTCCCTACACGACGCTCTTCCGATCTCAGCGAAAGAACAtNNNNNNNNNCGTCGCTA

GATCGGAAGAGCACACGTCTGAACTCCAGTCACTCGACGAATTCGGCC

RNA-seq U2OS-GR18 cells (Fig. 5C).

U2OS-GR18 cells were treated for 4h with either 1μM dexamethasone or 0.1% ethanol as vehicle control. RNA was isolated from 1.2 million cells using the RNeasy kit from Qiagen. Sequencing libraries were prepared using the TruSeq RNA library Prep Kit (Illumina). Prior to reverse transcription, poly adenylated RNA was isolated using oligo d(T) beads. Paired end 50bp reads from Illumina sequencing were mapped against the human hg19 reference genome using STAR [45] (options: --alignIntronMin 20 --alignIntronMax 500000 --chimSegmentMin 10 --outFilterMismatchNoverLmax 0.05 --outFilterMatchNmin 10 --outFilterScoreMinOverLread 0 --outFilterMatchNminOverLread 0 --outFilterMismatchNmax 10 --outFilterMultimapNmax 5). Differential gene expression between dex and etoh conditions from three biological replicates was calculated with DESeq2 [28], default parameters except betaPrior=FALSE.

Electrophoretic mobility shift assays

EMSAs were performed as described previously [3] using Cy-5 labeled oligos as listed in Table S2.

RNA isolation, reverse transcription and qPCR analysis

RNA was isolated from cells treated for either 4 h or overnight with 1 μM dexamethasone or with 0.1% ethanol vehicle. Total RNA was reverse transcribed using gene-specific primers for *GFP* (CAAACTCATCAATGTATCTTATCATG) and *RPL19* (GAGGCCAGTATGTACAGACAAAGTGG) which was used for data normalization. qPCR and data analysis were done as described [5]. Primer pairs for qPCR: hRPL19-fw: ATGTATCACAGCCTGTACCTG, hRPL19rev: TTCTTGGTCTCTTCCTCCTTG, GFP-fw: GGCCAGCTGTTGGGGTGTC, GFP-rev: TTGGGACAACTCCAGTGAAGA.

Noise-Measurements

For noise measurements, U2OS-GR18 cells were transfected using lipofectamine and plus (Invitrogen) essentially as described [5]. In short: The day before transfection, 40.000 U2OS-GR cells were seeded per well of a 24 well plate. The following day, cells were transfected with individual STARR reporter constructs (20ng/well) along with a SV-40 mCherry expression construct (20ng/well) and empty p6R plasmid (100 ng/ well). Transfected cells were treated overnight with either 1 μM dexamethasone or with 0.1% ethanol vehicle control. Fluorescence intensity was measured using an Accuri C6 flow cytometer (BD Biosciences) and the yellow laser (552nM) and filter 610/20 for mCherry and the deepblue laser (473nM) and filter 510/20 to measure GFP. Gates were set for mCherry and GFP and only cells showing both mCherry and GFP fluorescence were included in the analysis. Relative expression of GFP (GFP/Cherry), from 800-1600

526 individual dexamethasone-treated cells, was used to calculate mean expression and the
527 standard deviation of cell populations. Mean and standard deviation for noise (CV^2) and for
528 relative GFP expression were derived from three biological replicates.
529
530 **Computational analyses**
531 *Analysis of synSTARR-seq data*
532 RNA-seq reads were filtered and only sequences exactly matching the insert sequence in
533 length and nucleotide composition were included in the analysis. The number of
534 occurrences for each sequence variants was counted for each experimental condition and
535 differentially expressed sequences were identified using DESeq2 [28] using a p adjusted
536 value <0.01 as cut-off. To fit the dispersion curve to the mean distribution, we used the local
537 smoothed dispersion (DESeqwithfitType="local"). Notably, each of the constructs of the
538 flank libraries contains a functional GBS. Therefore, flanks that blunt activity will appear
539 repressed after hormone treated because their fraction in the total pool of sequences
540 decreases relative to flank variants with higher activities. For the flank libraries, we
541 obtained information for each sequence variant (1024) in the library. For the half site
542 library, we identified 61.582 out of the 65.536 possible variants present in this library. We
543 found that including sequences with low read coverage resulted in many false positive
544 differentially expressed GBS variants. To avoid this, we only included sequences with a
545 mean read count above 100 across all experiments, leaving us with information for 33.689
546 sequence variants. The pearson correlation coefficient for replicates was calculated using
547 the ggscatter function of the ggpubr library in R.

548 Boxplots comparing groups of sequence variants as specified in the figure legends show
549 center lines for the median; box limits indicate the 25th and 75th percentiles; whiskers
550 extend 1.5 times the interquartile range from the 25th and 75th percentiles.
551 Sequence logos to depict the consensus motif for groups of sequences were generated using
552 WebLogo [46]. The probability logo (activity motif) was generated with *k*pLogo [29] using
553 as input the sequence and fold change (dex/etoh) for each variant and the default settings
554 for weighted sequences.
555
556 *Motif weight*
557 The motif weight for each variant was calculated using the RSAT *matrix-scan* program [47,
558 48]. Specifically, the motif weight was calculated using Transfac motif M00205 truncated to
559 the core 15bp, and a custom background model created with RSAT *create background*
560 program, trained on human open chromatin available at UCSC genome browser
561 (http://genome.ucsc.edu/cgi-bin/hgTrackUi?db=hg19&g=wgEncodeRegDnaseClustered).
562 Boxplots comparing groups of sequence variants show center lines for the median; box
563 limits indicate the 25th and 75th percentiles; whiskers extend 1.5 times the interquartile
564 range from the 25th and 75th percentiles.
565
566 *Comparison of ChIP-seq peak height between combi2 and canonical GBS motif*
567 GR ChIP-seq data sets for U2OS-GR18 cells were downloaded as processed peaks from EBI
568 ArrayExpress (E-MTAB-2731). ChIP-seq peaks in a 40 kb window centered on the
569 transcription start site of differentially expressed genes (RNA-seq data: E-MTAB-6738)
570 were scanned using RSAT *matrix-scan* [47, 48] for the occurrence of either a GBS-match
571 (Transfac matrix M00205, p value cut-off: 10^{-4}) or the combi2 matrix we generated (Fig. 5D,

572 p-value cut-off 10^{-4}). Next, peaks were grouped by motif match and median peak height was
573 calculated for each group and the p-value comparing both groups was calculated using a
574 Wilcoxon rank-sum test to produce Supplementary Fig. S8B.
575
576 *Comparison of gene regulation*
577 To compare the level of activation between genes with nearby peaks with either a GBS
578 match (Transfac matrix M00205, p value cut-off: 10^{-4}) or a combi2 match (motif Fig. 5D, p-
579 value cut-off 10^{-4}), we first scanned ChIP-seq peaks (U2OS-GR cells: E-MTAB-2731) in a 40
580 kb window centered on the transcription start site (using all annotated TSSs from Ensembl
581 GRCH37) for motif matches using RSAT *matrix-scan* [47, 48]. Only peaks with an exclusive
582 motif match were retained to generate a boxplot comparing the log2 fold change for genes
583 of each group (RNA-seq data: E-MTAB-2731). Center lines show the median, box limits
584 indicating the 25th and 75th percentiles and whiskers extending 1.5 times the interquartile
585 range from the 25th and 75th percentiles. p-value comparing the log2 fold change for both
586 groups was calculated using a Wilcoxon rank-sum test to produce figure 5C.
587
588 *DNA shape prediction*
589 We used DNAshapeR [31] to predict the minor groove width for sequence variants of
590 interest. Boxplots for individual nucleotide position show center lines for the median; box
591 limits indicate the 25th and 75th percentiles; whiskers extend 1.5 times the interquartile
592 range from the 25th and 75th percentiles. The Wilcoxon rank-sum test was used to
593 calculate the p-values comparing nucleotide position variants between groups. Individual
594 sites were clustered using K-means clustering with k=4 clusters nstart=20 and 100 restarts
595 with the function 'kmeans' from the R 'stats' package.

596

597 *Classification of GBS activity*

598 To assess classifier performance we generate ROC curves using 10-fold cross-validation.
599 Four different models were tested to classify GBS activity into blunting or enhancing. A
600 mononucleotide model consisting of sequence motifs estimated from relative nucleotide
601 frequencies within the two classes. Class affiliation is predicted with a likelihood ratio test.
602 We also tested a similar model based on dinucleotides. In addition, we tested two random
603 forest (RF) classifiers with 100 trees, based on sequence and shape information. We used
604 the R package "randomForest" for constructing the classifiers [49]. Since RF classifiers are
605 not designed for categorical data, we coded nucleotide sequences using 00 for 'A', 01 for 'C',
606 10 for 'G', and 11 for 'T'.

607

608 *ChIP-exo footprint profiles*

609 ChIP-exo footprint profiles were generated using the ExoProfiler package [32] and
610 published ChIP-exo (EBI ArrayExpress E-MTAB-2955) and ChIP-seq (E-MTAB-2956) data
611 for IMR90 cells as input. Peaks were scanned using either the JASPAR MA0113.2 motif [50],
612 the PWM for the combi1 motif [32], the combi2 motif (Fig. 5D) or for the AC flank variant,
613 the motif depicted in figure S4A. Hits were included if the p-value was $<10^{-4}$. Overlay plots
614 for distinct motifs were generated by aligning the profiles on the GBS and normalizing the
615 signal for each motif variant to 1.

616

617 *Structural alignment of GR:ETS1 complex*

618 Structural alignment of the GR:ETS1 complex on a combi2 sequence was done as described
619 previously [32] except that both GR dimer halves are retained in the resulting model. In

620 short: A structural model of the DNA hybrid sequence (AGAACATTCCGGCACT) was
621 generated using 3D-Dart [51] using the ETS1 structure (PDB entry 1K79) and the GR
622 structure (PDB entry 3G6U). GR and the ETS2 binding motifs were aligned using the CE-
623 align algorithm [52] to the 3D-DART DNA model of the hybrid sequence.
624
625 **Data access**
626 Data were deposited in ArrayExpress under the accession numbers: E-MTAB-6738 (RNA-
627 seq U2OS-GR18) and E-MTAB-6737 (synSTARR-seq U2OS-GR18). In addition, we used the
628 previously deposited datasets: E-MTAB-2731 (ChIP-seq U2OS cells), E-MTAB-2955 and E-
629 MTAB-2956 (ChIP-seq and ChIP-exo data IMR90).
630
631 **Reviewers access to datasets:**
632 STARR-seq data: E-MTAB-6737
633 Username: Reviewer_E-MTAB-6737
634 Password: hgeofcho
635 RNA-seq data: E-MTAB-6738
636 Username: Reviewer_E-MTAB-6738
637 Password: cieef7tt
638
639 *Funding*
640 This work was supported by the Deutsche Forschungsgemeinschaft [ME4154/1-1 to SS and
641 MJ].
642
643

Acknowledgements

We would like to thank Marcel Jurk for performing the structural alignment presented.

Author's contributions

S.S., M.B., M.B., M.T.C., E.E., P.B. and S.H.M. performed and conceived experiments and analyzed the data. S.S., M.T.C., M.V. and S.H.M. designed and supervised the study and wrote the manuscript with input from all authors.

References

1. Grossman SR, Zhang X, Wang L, Engreitz J, Melnikov A, Rogov P, Tewhey R, Isakova A, Deplancke B, Bernstein BE, et al: **Systematic dissection of genomic features determining transcription factor binding and enhancer function.** *Proc Natl Acad Sci U S A* 2017, **114:**E1291-E1300.
2. Schmid W, Strahle U, Schutz G, Schmitt J, Stunnenberg H: **Glucocorticoid receptor binds cooperatively to adjacent recognition sites.** *EMBO J* 1989, **8:**2257-2263.
3. Schone S, Jurk M, Helabad MB, Dror I, Lebars I, Kieffer B, Imhof P, Rohs R, Vingron M, Thomas-Chollier M, Meijsing SH: **Sequences flanking the core-binding site modulate glucocorticoid receptor structure and activity.** *Nat Commun* 2016, **7:**12621.
4. Watson LC, Kuchenbecker KM, Schiller BJ, Gross JD, Pufall MA, Yamamoto KR: **The glucocorticoid receptor dimer interface allosterically transmits sequence-specific DNA signals.** *Nat Struct Mol Biol* 2013, **20:**876-883.
5. Meijsing SH, Pufall MA, So AY, Bates DL, Chen L, Yamamoto KR: **DNA binding site sequence directs glucocorticoid receptor structure and activity.** *Science* 2009, **324:**407-410.

6. Maheshri N, O'Shea EK: **Living with noisy genes: how cells function reliably with inherent variability in gene expression.** *Annu Rev Biophys Biomol Struct* 2007, **36:**413-434.

7. Blake WJ, M KA, Cantor CR, Collins JJ: **Noise in eukaryotic gene expression.** *Nature* 2003, **422:**633-637.

8. Kaern M, Elston TC, Blake WJ, Collins JJ: **Stochasticity in gene expression: from theories to phenotypes.** *Nat Rev Genet* 2005, **6:**451-464.

9. Raj A, van Oudenaarden A: **Single-molecule approaches to stochastic gene expression.** *Annu Rev Biophys* 2009, **38:**255-270.

10. Ross IL, Browne CM, Hume DA: **Transcription of individual genes in eukaryotic cells occurs randomly and infrequently.** *Immunol Cell Biol* 1994, **72:**177-185.

11. Suter DM, Molina N, Gatfield D, Schneider K, Schibler U, Naef F: **Mammalian genes are transcribed with widely different bursting kinetics.** *Science* 2011, **332:**472-474.

12. Fritzsch C, Baumgartner S, Kuban M, Steinshorn D, Reid G, Legewie S: **Estrogen-dependent control and cell-to-cell variability of transcriptional bursting.** *Mol Syst Biol* 2018, **14:**e7678.

13. Cai L, Friedman N, Xie XS: **Stochastic protein expression in individual cells at the single molecule level.** *Nature* 2006, **440:**358-362.

14. Raser JM, O'Shea EK: **Control of stochasticity in eukaryotic gene expression.** *Science* 2004, **304:**1811-1814.

15. Blake WJ, Balazsi G, Kohanski MA, Isaacs FJ, Murphy KF, Kuang Y, Cantor CR, Walt DR, Collins JJ: **Phenotypic consequences of promoter-mediated transcriptional noise.** *Mol Cell* 2006, **24:**853-865.

16. Sharon E, van Dijk D, Kalma Y, Keren L, Manor O, Yakhini Z, Segal E: **Probing the effect of promoters on noise in gene expression using thousands of designed sequences.** *Genome Res* 2014, **24:**1698-1706.

17. Hornung G, Bar-Ziv R, Rosin D, Tokuriki N, Tawfik DS, Oren M, Barkai N: **Noise-mean relationship in mutated promoters.** *Genome Res* 2012, **22:**2409-2417.

18. Dey SS, Foley JE, Limsirichai P, Schaffer DV, Arkin AP: **Orthogonal control of expression mean and variance by epigenetic features at different genomic loci.** *Mol Syst Biol* 2015, **11:**806.

19. Dadiani M, van Dijk D, Segal B, Field Y, Ben-Artzi G, Raveh-Sadka T, Levo M, Kaplow I, Weinberger A, Segal E: **Two DNA-encoded strategies for increasing expression with opposing effects on promoter dynamics and transcriptional noise.** *Genome Res* 2013, **23:**966-976.

20. Raser JM, O'Shea EK: **Noise in gene expression: origins, consequences, and control.** *Science* 2005, **309:**2010-2013.

21. Inoue F, Ahituv N: **Decoding enhancers using massively parallel reporter assays.** *Genomics* 2015, **106:**159-164.

22. Arnold CD, Gerlach D, Stelzer C, Boryn LM, Rath M, Stark A: **Genome-wide quantitative enhancer activity maps identified by STARR-seq.** *Science* 2013, **339:**1074-1077.

23. Liu Y, Yu S, Dhiman VK, Brunetti T, Eckart H, White KP: **Functional assessment of human enhancer activities using whole-genome STARR-sequencing.** *Genome Biol* 2017, **18:**219.

24. Vanhille L, Griffon A, Maqbool MA, Zacarias-Cabeza J, Dao LT, Fernandez N, Ballester B, Andrau JC, Spicuglia S: **High-throughput and quantitative assessment of enhancer activity in mammals by CapStarr-seq.** *Nat Commun* 2015, **6:**6905.

25. Vockley CM, D'Ippolito AM, McDowell IC, Majoros WH, Safi A, Song L, Crawford GE, Reddy TE: **Direct GR Binding Sites Potentiate Clusters of TF Binding across the Human Genome.** *Cell* 2016, **166:**1269-1281 e1219.

26. Shlyueva D, Stelzer C, Gerlach D, Yanez-Cuna JO, Rath M, Boryn LM, Arnold CD, Stark A: **Hormone-responsive enhancer-activity maps reveal predictive motifs, indirect repression, and targeting of closed chromatin.** *Mol Cell* 2014, **54:**180-192.

27. Rogatsky I, Trowbridge JM, Garabedian MJ: **Glucocorticoid receptor-mediated cell cycle arrest is achieved through distinct cell-specific transcriptional regulatory mechanisms.** *Mol Cell Biol* 1997, **17:**3181-3193.

28. Love MI, Huber W, Anders S: **Moderated estimation of fold change and dispersion for RNA-seq data with DESeq2.** *Genome Biol* 2014, **15:**550.

29. Wu X, Bartel DP: **kpLogo: positional k-mer analysis reveals hidden specificity in biological sequences.** *Nucleic Acids Res* 2017, **45:**W534-W538.

30. Zhang L, Martini GD, Rube HT, Kribelbauer JF, Rastogi C, FitzPatrick VD, Houtman JC, Bussemaker HJ, Pufall MA: **SelexGLM differentiates androgen and glucocorticoid receptor DNA-binding preference over an extended binding site.** *Genome Res* 2018, **28:**111-121.

31. Chiu TP, Comoglio F, Zhou T, Yang L, Paro R, Rohs R: **DNAshapeR: an R/Bioconductor package for DNA shape prediction and feature encoding.** *Bioinformatics* 2016, **32:**1211-1213.

32. Starick SR, Ibn-Salem J, Jurk M, Hernandez C, Love MI, Chung HR, Vingron M, Thomas-Chollier M, Meijsing SH: **ChIP-exo signal associated with DNA-binding motifs provides insight into the genomic binding of the glucocorticoid receptor and cooperating transcription factors.** *Genome Res* 2015, **25:**825-835.

33. Rhee HS, Pugh BF: **Comprehensive genome-wide protein-DNA interactions detected at single-nucleotide resolution.** *Cell* 2011, **147:**1408-1419.

34. Strahle U, Schmid W, Schutz G: **Synergistic action of the glucocorticoid receptor with transcription factors.** *EMBO J* 1988, **7:**3389-3395.

35. Pearce D, Yamamoto KR: **Mineralocorticoid and glucocorticoid receptor activities distinguished by nonreceptor factors at a composite response element.** *Science* 1993, **259:**1161-1165.

36. Yang L, Orenstein Y, Jolma A, Yin Y, Taipale J, Shamir R, Rohs R: **Transcription factor family-specific DNA shape readout revealed by quantitative specificity models.** *Mol Syst Biol* 2017, **13:**910.

741 37. Rohs R, Jin X, West SM, Joshi R, Honig B, Mann RS: **Origins of specificity in protein-DNA**
742 **recognition.** *Annu Rev Biochem* 2010, **79:**233-269.
743 38. Abe N, Dror I, Yang L, Slattery M, Zhou T, Bussemaker HJ, Rohs R, Mann RS: **Deconvolving the**
744 **recognition of DNA shape from sequence.** *Cell* 2015, **161:**307-318.
745 39. Zheng J, Chang MR, Stites RE, Wang Y, Bruning JB, Pascal BD, Novick SJ, Garcia-Ordonez RD,
746 Stayrook KR, Chalmers MJ, et al: **HDX reveals the conformational dynamics of DNA sequence**
747 **specific VDR co-activator interactions.** *Nat Commun* 2017, **8:**923.
748 40. Zhang J, Chalmers MJ, Stayrook KR, Burris LL, Wang Y, Busby SA, Pascal BD, Garcia-Ordonez RD,
749 Bruning JB, Istrate MA, et al: **DNA binding alters coactivator interaction surfaces of the intact**
750 **VDR-RXR complex.** *Nat Struct Mol Biol* 2011, **18:**556-563.
751 41. Hall JM, McDonnell DP, Korach KS: **Allosteric regulation of estrogen receptor structure,**
752 **function, and coactivator recruitment by different estrogen response elements.** *Mol Endocrinol*
753 2002, **16:**469-486.
754 42. Parker SC, Hansen L, Abaan HO, Tullius TD, Margulies EH: **Local DNA topography correlates with**
755 **functional noncoding regions of the human genome.** *Science* 2009, **324:**389-392.
756 43. Mathelier A, Xin B, Chiu TP, Yang L, Rohs R, Wasserman WW: **DNA Shape Features Improve**
757 **Transcription Factor Binding Site Predictions In Vivo.** *Cell Syst* 2016, **3:**278-286 e274.
758 44. Singh A, Razooky B, Cox CD, Simpson ML, Weinberger LS: **Transcriptional bursting from the HIV-**
759 **1 promoter is a significant source of stochastic noise in HIV-1 gene expression.** *Biophys J* 2010,
760 **98:**L32-34.
761 45. Dobin A, Davis CA, Schlesinger F, Drenkow J, Zaleski C, Jha S, Batut P, Chaisson M, Gingeras TR:
762 **STAR: ultrafast universal RNA-seq aligner.** *Bioinformatics* 2013, **29:**15-21.
763 46. Crooks GE, Hon G, Chandonia JM, Brenner SE: **WebLogo: a sequence logo generator.** *Genome*
764 *Res* 2004, **14:**1188-1190.

47. Thomas-Chollier M, Defrance M, Medina-Rivera A, Sand O, Herrmann C, Thieffry D, van Helden J: **RSAT 2011: regulatory sequence analysis tools.** *Nucleic Acids Res* 2011, **39:**W86-91.

48. Turatsinze JV, Thomas-Chollier M, Defrance M, van Helden J: **Using RSAT to scan genome sequences for transcription factor binding sites and cis-regulatory modules.** *Nat Protoc* 2008, **3:**1578-1588.

49. Wiener ALaM: **Classification and Regression by randomForest.** *R News* 2002, **2:**18-22.

50. Khan A, Fornes O, Stigliani A, Gheorghe M, Castro-Mondragon JA, van der Lee R, Bessy A, Cheneby J, Kulkarni SR, Tan G, et al: **JASPAR 2018: update of the open-access database of transcription factor binding profiles and its web framework.** *Nucleic Acids Res* 2018, **46:**D260-D266.

51. van Dijk M, Bonvin AM: **3D-DART: a DNA structure modelling server.** *Nucleic Acids Res* 2009, **37:**W235-239.

52. Jia Y, Dewey TG, Shindyalov IN, Bourne PE: **A new scoring function and associated statistical significance for structure alignment by CE.** *J Comput Biol* 2004, **11:**787-799.

Figure legends

Figure 1. Design and validation of the synSTARR-seq approach. (a) SynSTARR-seq reporter setup using a synthetic library containing a GR Binding Sequence (GBS) flanked by 1024 different flanking sequences (flank library) to screen for flanks that modulate GBS activity. Samples are treated with dexamethasone (dex) or ethanol vehicle (etoh) before targeted RNA-sequencing and counting of the reads. (b) Transcriptional activation of STARR-seq reporter containing candidate enhancer inserts as indicated. Mean fold change upon dexamethasone treatment ± S.D. (n = 3) in U2OS-GR18 cells is shown. Genomic

FKBP5 (211bp region hg19Chr6: 35699789-35699999); FKBP5-2 GBS (single GBS: AGAACAtccTGTGCC); no GBS (AGAAACtccGTTGCC). (c) Representative RNA-seq correlation plot for biological replicates of dexamethasone-treated cells (4h, 1µM) transfected with the GBS-flank library. (d) The enhancer activity of blunting (n=5), neutral (n=5) and enhancing (n=5) flank variants was assessed for individually transfected STARR-seq constructs by qPCR. Fold change upon dexamethasone treatment normalized to the activity for the scrambled control plasmid is shown as horizontal line for the mean of each activity group and as dot for each individual construct.

Figure 2. Analysis of the GBS flank library. (a) Color chart summarizing the sequence at each variable position for flank variants ranked by their fold change in response to hormone treatment. (b) Consensus motif for (top) significantly (adjusted p-value < 0.01) enhancing and (bottom) blunting flank variants. (c) *k*pLogo probability logo (activity logo) for flank variants depicting the p-values from Mann-Whitney U tests of whether GBS variants with a specific nucleotide at a given position are more (displayed above number indicating nucleotide position) or less (displayed below number indicating nucleotide position) active than other GBS variants. Positions with significant nucleotides ($p < 0.001$) are highlighted (red coordinates). (d) Transcriptional activity of STARR-seq reporters containing candidate flank variants as indicated. Relative RNA levels ± S.E.M. are shown for cells treated with ethanol vehicle and for cells treated overnight with 1 µM dexamethasone ($n \geq 3$). (e) Table of EMSA-derived DNA-binding constants (Kd) for flank variants as indicated ± S.D. ($n \geq 3$).

Figure 3. Predicted DNA shape for enhancing and blunting flank variants. (a) Predicted minor groove width (MGW) for significant enhancing and blunting flank variants of the Cgt GBS library ranked by their fold change in response to hormone treatment. (b) K-means clustering based on MGW for significantly enhancing and blunting flank variants. Right side: activating and blunting variants are highlighted in grey and black respectively. (c) Log2 fold change upon dexamethasone treatment for each cluster as

814 indicated. The synSTARR-seq activity for individual sequences is shown as black dots, the median for each
815 cluster as a horizontal red line. (d) Consensus sequence motif for clusters as indicated.
816
817 **Figure 4. Analysis of the GBS half site library.** (a) SynSTARR-seq reporter setup using a synthetic library
818 containing 65536 candidate GR Binding Sequence (GBS) variants (half site library with 8 variable positions
819 N). (b) Candidate GBS variants were ranked by their fold change in expression in response to hormone
820 treatment (4 h, 1 µM dex). Only sequences with a mean read count > 100 across all replicates (n=3) for
821 both dex and ethanol vehicle treated cells are shown. Repressed (log2 FC < -2), weakly active (0 < log2 FC
822 <2) and activated GBS variants (log2 FC ≥ 2) are highlighted by a blue, green and red background
823 respectively. (c) The enhancer activity of negative (n=4), weak (n=4) and strong (n=8) GBS variants was
824 assessed by qPCR for individually transfected STARR-seq constructs. Fold change upon dexamethasone
825 treatment normalized to the activity for the scrambled control plasmid is shown. Horizontal line shows
826 the mean for each activity group; dots the values for individual constructs. (d) Top: Consensus motif and
827 below a color chart summarizing the sequence at each variable position for each significantly activated
828 GBS variant (adjusted p-value < 0.01) ranked by their fold change in response to dex treatment. (e)
829 *k*pLogo probability logo (activity logo) for half site variants depicting the p-values from Mann-Whitney U
830 tests of whether GBS variants with a specific nucleotide at a given position are more (displayed above
831 number indicating nucleotide position) or less (displayed below number indicating nucleotide position)
832 active than other GBS variants. Positions with significant nucleotides (p < 0.001) are highlighted in red,
833 fixed positions in black. (f) Log2 fold change upon dexamethasone treatment for GBS-like variants with
834 either an A, C, G or T at position 2 (exact match to AGAACATnnXGTnCn, with X either A,C,G or T). Data for
835 individual sequences are shown as blue dots. Horizontal red lines show the median for each group. p-
836 values were calculated using a Student's t-test. (g) Boxplot of the motif weight (using the truncated 15nt
837 long M00205 motif from Transfac) for inactive (-0.5≤ log2 fold change ≤0.5; white), active (light red) and
838 the top 10% active (dark red) GBS variants. p-values were calculated using a Student's t-test.

Figure 5. Identification and characterization of the combi2 motif. (a) Color chart for the top activated GBS variants and above the consensus motif for the 25 most active sequences (b) Transcriptional activity of STARR-seq reporters containing candidate GBS variants as indicated. Relative RNA levels ± S.E.M. are shown for cells treated with ethanol vehicle and for cells treated overnight with 1 µM dexamethasone (n = 3). (c) Boxplot of the log2 fold change upon treatment for 4 h with 1 µM dexamethasone for genes with a ChIP-seq peak in the region ±20 kb around the TSS containing either a conventional GBS match (M00205; p value <0.0001) or a combi2-like sequence (combi2 motif; p value < 0.0001). Center lines show the median. p-value was calculated using the Wilcoxon rank sum test. (d) Motif logo representing the positional weight matrices for the canonical GBS (JASPAR MA0113.2), combi1 and combi2 motif. (e) Alignment of the ChIP-exo footprint profiles for the combi2 and the conventional GBS motif. Arrows 1 and 2: Additional 5' coverage for the combi2 motif that does not match the conventional GBS footprint. (f) Alignment of the ChIP-exo footprint profiles for the combi1 and combi2 motif. Arrows 1 and 2: Additional 5' coverage for the combi2 motif when compared to the GBS footprint aligns with signal for the combi1 footprint. (g) Structural alignment of combined binding of a GR dimer (green) and ETS1 (purple, middle: PDB 1K79) at the combi2 sequence (orange).

Figure 6. The effect of GBS sequence, number and presence of other TFBS on transcriptional output and noise. (a) Mean GFP expression relative to mCherry of the STARR-seq reporter for cell populations treated overnight with 1 µM dexamethasone with binding site variant as indicated was determined by flow cytometry. (b) The single-cell distribution of GFP expression relative to co-transfected mCherry was determined for each binding site variant as indicated by flow cytometry. The mean and noise for each binding site variant are extracted from these distributions (see Methods). (c) Average and S.D. for mean GFP expression and for noise from three biological replicates. Area with mostly single GBS variants is highlighted with a blue background; Area with three GBSs with a green background and area with

composite binding sites consisting of a single GBS and a binding site for another TF with a red background.

Supplementary figure legends

Figure S1. Analysis of individual enhancer variants by flow cytometry and synSTARR-seq reproducibility. (a) Analysis of individual enhancer variants as indicated by flow cytometry showing the side scatter (SSC-A) versus GFP signal for individual mCherry-positive cells. Left: no STARR-seq construct. Right-Top: ethanol, vehicle, treated cells; Right-Bottom: Cells treated overnight with 1µM dexamethasone. Numbers in red indicate the percentage of GFP+ (top right side) and GFP- (top left side) cells respectively. Red vertical line demarcates the threshold for being called GFP+. (b) RNA-seq correlation plots for biological replicates of vehicle-treated cells transfected with the GBS-flank library (Cgt flank library). (c) Same as (b) except for biological replicates of dexamethasone-treated cells (4h 1µM). (d) RNA-seq correlation plots for biological replicates of vehicle-treated cells transfected with the GBS-flank library (Sgk flank library). (e) Same as (d) except for biological replicates of dexamethasone-treated cells (4h 1µM).

Figure S2. Analysis of the Sgk flank library. (a) Color chart summarizing the sequence at each variable position for flank variants ranked by their fold change in response to hormone treatment. (b) Consensus motif for (left) significantly enhancing and (right) blunting flank variants (c) *k*pLogo probability logo (activity logo) for flank variants depicting the p-values from Mann-Whitney U tests of whether GBS variants with a specific nucleotide at a given position are more (displayed above number indicating nucleotide position) or less (displayed below number indicating nucleotide position) active than other GBS variants. Positions with significant nucleotides ($p < 0.001$) are highlighted (red coordinates). (d) Predicted minor groove width (MGW) for significant enhancing and blunting flank variants of the Sgk GBS

889 library ranked by their fold change in response to hormone treatment. (e) K-means clustering based on
890 MGW for significantly enhancing and blunting flank variants. Right side: activating and blunting variants
891 are highlighted in grey and black respectively. (e) Consensus sequence motif for clusters as indicated. (g)
892 Log2 fold change upon dexamethasone treatment for each cluster as indicated. The synSTARR-seq
893 activity for individual sequences is shown as black dots, the median for each group as a horizontal red
894 line.
895
896 **Figure S3. MGW comparison between blunting and enhancing flanks.** (a) Minor groove width (MGW)
897 for selected individual bases for significantly blunting (n=189) and significantly enhancing (n=125) flanks
898 for the Cgt library. p-values were calculated using the Wilcoxon rank-sum test. (b) Same as for (a) except
899 for significantly blunting (n=162) and significantly enhancing (n=101) flanks of the Sgk flank library.
900
901 **Figure S4. Analysis of the nACnn flank.** (a) Motif logo representing the positional weight matrix of highly
902 active flank variants that was used to scan for motif-matches to generate the ChIP-exo footprint profile.
903 (b) Alignment of the ChIP-exo footprint profiles for highly active flank variant matches (p value <0.0001;
904 solid lines: blue: positive strand, red: negative strand) and for the conventional GBS motif (M00205; p
905 value <0.0001; shaded areas; blue: positive strand, red: negative strand).
906
907 **Figure S5. synSTARR-seq reproducibility for the half site library.** (a) Correlation plot between input
908 library (library) and the plasmid library isolated from transfected U2OS-GR18 cells (input). (b) RNA-seq
909 correlation plots for biological replicates of vehicle-treated cells. (c) Same as for (b) except for biological
910 replicates of dexamethasone-treated cells (4h 1µM).
911
912 **Figure S6. Effect of spacer sequence on GBS activity**. (a) Motif logo representing the sequence that was
913 used to scan for GBS-matches in the half site library. Black box highlights the two positions in the spacer

914 whose effect on GBS activity was assayed. (b) Boxplot of the log2 fold change upon treatment for 4 h
915 with 1 µM dexamethasone for GBS matches with spacer variant as indicated. Center lines show the
916 median. The Benjamini-Hochberg corrected p-value for the spacer variants with the most significance
917 difference was calculated using a Student's t-test.
918
919 **Figure S7. Analysis of the GBS half site library**. (a) Log2 fold change upon dexamethasone treatment for
920 active GBS variants with either an A, C, G or T at position 3. Data for individual sequences that match
921 consensus second half site at key positions 4 and 6 (exact match to AGAACATnnnXTnCn, with X either
922 A,C,G or T) are shown as blue dots. Horizontal red lines show the average for each group. p-value was
923 calculated using a Student's t-test. (b) Left: Minor groove width (MGW) prediction for GBS variants
924 ranked by activity. Right: Consensus motif for top 20% most active and bottom 20% least active GBS
925 variants. (c) MGW for select individual bases comparing the top 20% most active and bottom 20% least
926 active activated GBS variants. p-values were calculated using the Wilcoxon rank-sum test.
927
928 **Figure S8. Characterization of the combi2 motif.** (a) Transcriptional activity of STARR-seq reporters
929 containing candidate GBS variants as indicated. Relative RNA levels ± S.E.M. are shown for cells treated
930 with ethanol vehicle and for cells treated overnight with 1 µM dexamethasone (n = 3). (b) Boxplot
931 showing the peak-height for GR target genes with either a canonical GBS motif match (nnTGT) or a
932 combi2 motif match (tcCGT). Center lines show the median, p value was calculated using a Wilcoxon
933 rank-sum test.
934
935 **Figure S9. Prediction of GBS activity based on DNA sequence or DNA shape.** (a) ROC curves analyzing
936 the ability of the models to distinguish between blunting and enhancing flank variants for (left) the Cgt
937 flank library; (right) the Sgk flank library. Mononucleotide: Classifier based on mononucleotide
938 frequencies within the two classes. Dinucleotide: Classifier constructed using dinucleotide frequencies.

939 Sequence Random Forest (RF): Random Forest classifer trained and tested on coded nucleotide
940 sequences. Shape Random Forest (RF): Random forest classifier based on predicted MGW. (b) Same as
941 for (a) except that model and ROC curves where trained and assessed for their ability to discriminate
942 between the top and bottom 20% significantly active GBS variants from the half site library.
943

Synthetic STARR-seq reveals how DNA shape and sequence modulate transcriptional output and noise.

Stefanie Schöne[1], Melissa Bothe[1], Edda Einfeldt[1], Marina Borschiwer[1], Philipp Benner[1], Martin Vingron[1], Morgane Thomas-Chollier[2], Sebastiaan H. Meijsing[1]

[1] *Max Planck Institute for Molecular Genetics, Ihnestraße 63-67, 14195 Berlin, Germany.*
[2] *Institut de biologie de l'Ecole normale supérieure (IBENS), Ecole normale supérieure, CNRS, INSERM, PSL Université Paris, 75005 Paris, France.*

Contact information:

Sebastiaan H. Meijsing
Max Planck Institute for Molecular Genetics,
Ihnestrasse 63-73
14195, Berlin, Germany
Tel: +49-30-84131176
Email: meijsing@molgen.mpg.de

Figures

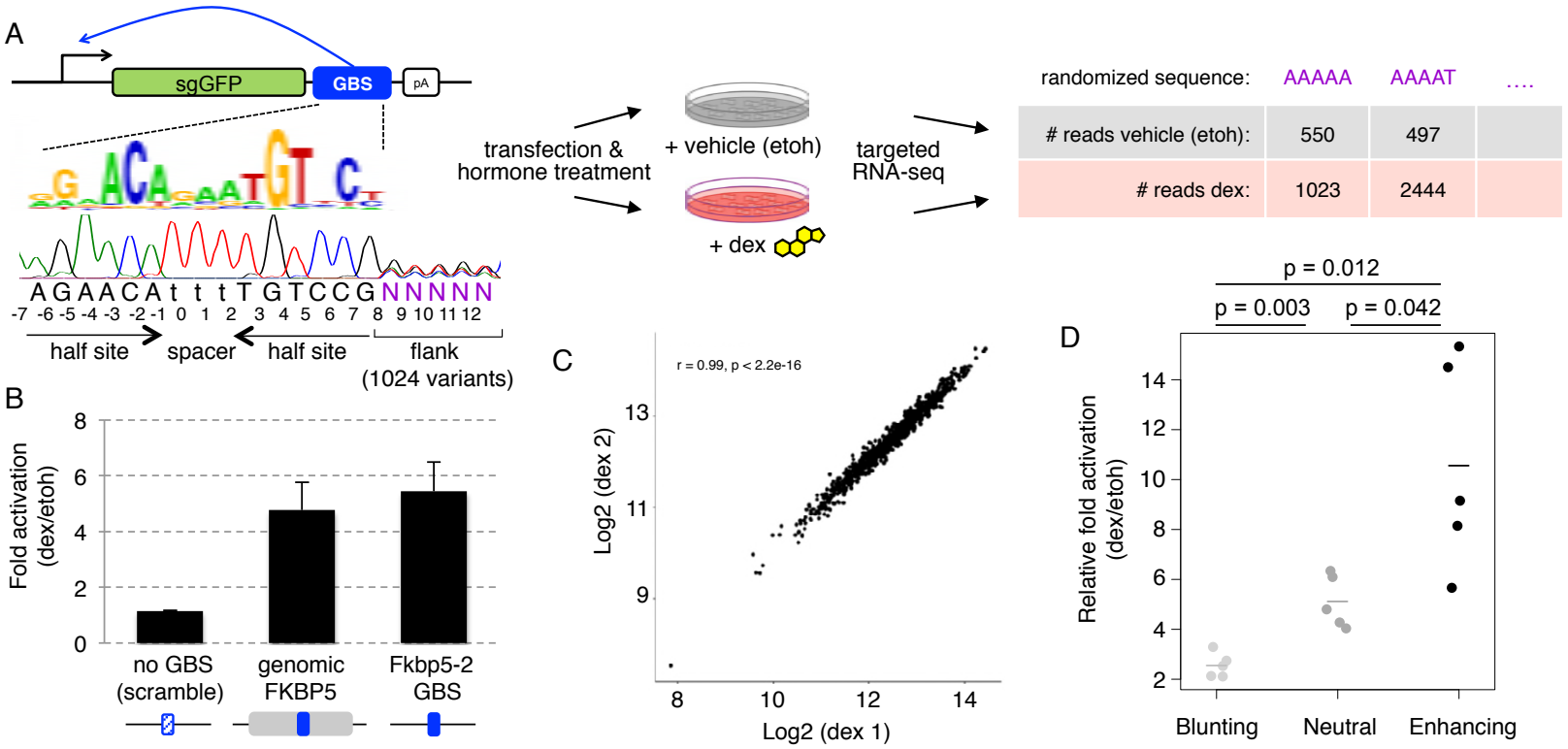

Figure 1. Design and validation of the synSTARR-seq approach. (a) SynSTARR-seq reporter setup using a synthetic library containing a GR Binding Sequence (GBS) flanked by 1024 different flanking sequences (flank library) to screen for flanks that modulate GBS activity. Samples are treated with dexamethasone (dex) or ethanol vehicle (etoh) before targeted RNA-sequencing and counting of the reads. (b) Transcriptional activation of STARR-seq reporter containing candidate enhancer inserts as indicated. Mean fold change upon dexamethasone treatment ± S.D. (n = 3) in U2OS-GR18 cells is shown. Genomic FKBP5 (211bp region hg19Chr6: 35699789-35699999); FKBP5-2 GBS (single GBS: AGAACAtccTGTGCC); no GBS (AGAAACtccGTTGCC). (c) Representative RNA-seq correlation plot for biological replicates of dexamethasone-treated cells (4h, 1μM) transfected with the GBS-flank library. (d) The enhancer activity of blunting (n=5), neutral (n=5) and enhancing (n=5) flank variants was assessed for individually transfected STARR-seq constructs by qPCR. Fold change upon dexamethasone treatment normalized to the activity for the scrambled control plasmid is shown as horizontal line for the mean of each activity group and as dot for each individual construct.

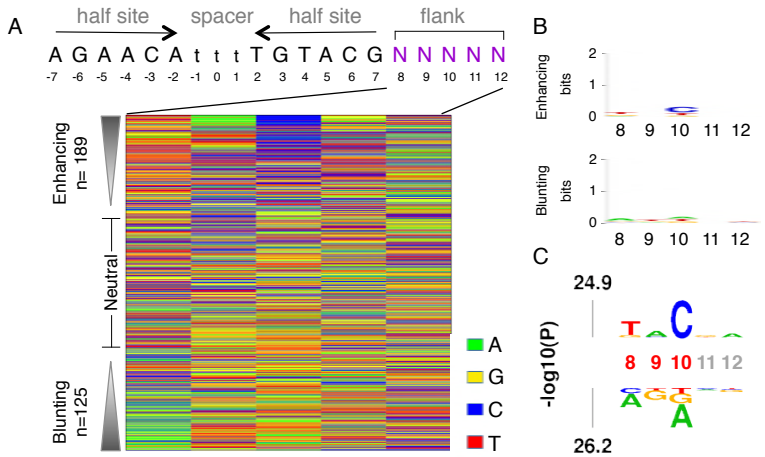

E

Effect:	flank seq.:	Kd (μM):	S.D.:
enhancing	TACGT	0.41	0.07
neutral	TCAGT	0.63	0.22
blunting-1	CATGT	0.42	0.13
blunting-2	ATTTT	0.24	0.11

Figure 2. Analysis of the GBS flank library. (a) Color chart summarizing the sequence at each variable position for flank variants ranked by their fold change in response to hormone treatment. (b) Consensus motif for (top) significantly (adjusted p-value < 0.01) enhancing and (bottom) blunting flank variants. (c) *k*pLogo probability logo (activity logo) for flank variants depicting the p-values from Mann-Whitney U tests of whether GBS variants with a specific nucleotide at a given position are more (displayed above number indicating nucleotide position) or less (displayed below number indicating nucleotide position) active than other GBS variants. Positions with significant nucleotides ($p < 0.001$) are highlighted (red coordinates). (d) Transcriptional activity of STARR-seq reporters containing candidate flank variants as indicated. Relative RNA levels ± S.E.M. are shown for cells treated with ethanol vehicle and for cells treated overnight with 1 μM dexamethasone ($n \geq 3$). (e) Table of EMSA-derived DNA-binding constants (Kd) for flank variants as indicated ± S.D. ($n \geq 3$).

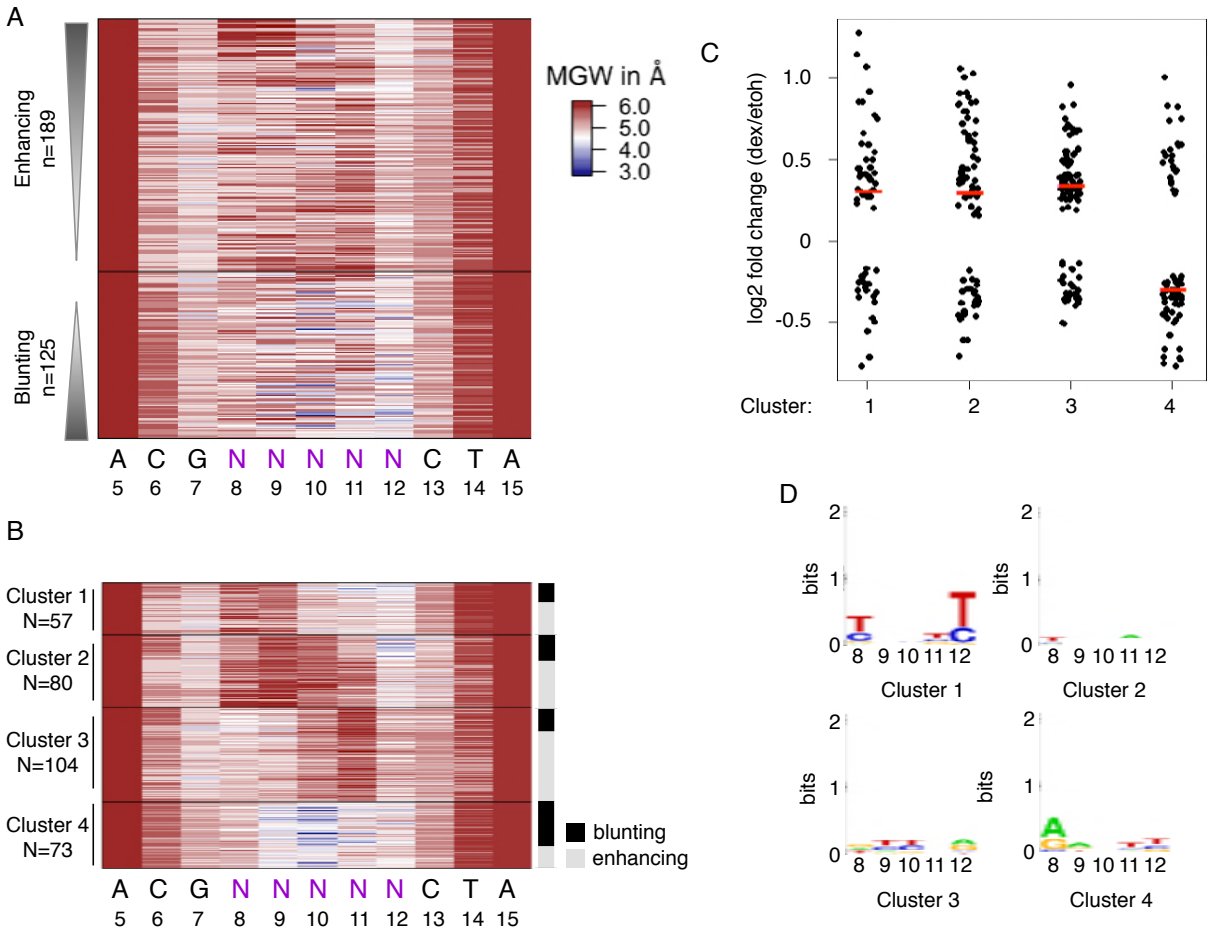

Figure 3. Predicted DNA shape for enhancing and blunting flank variants. (a) Predicted minor groove width (MGW) for significant enhancing and blunting flank variants of the Cgt GBS library ranked by their fold change in response to hormone treatment. (b) K-means clustering based on MGW for significantly enhancing and blunting flank variants. Right side: activating and blunting variants are highlighted in grey and black respectively. (c) Log2 fold change upon dexamethasone treatment for each cluster as indicated. The synSTARR-seq activity for individual sequences is shown as black dots, the median for each cluster as a horizontal red line. (d) Consensus sequence motif for clusters as indicated.

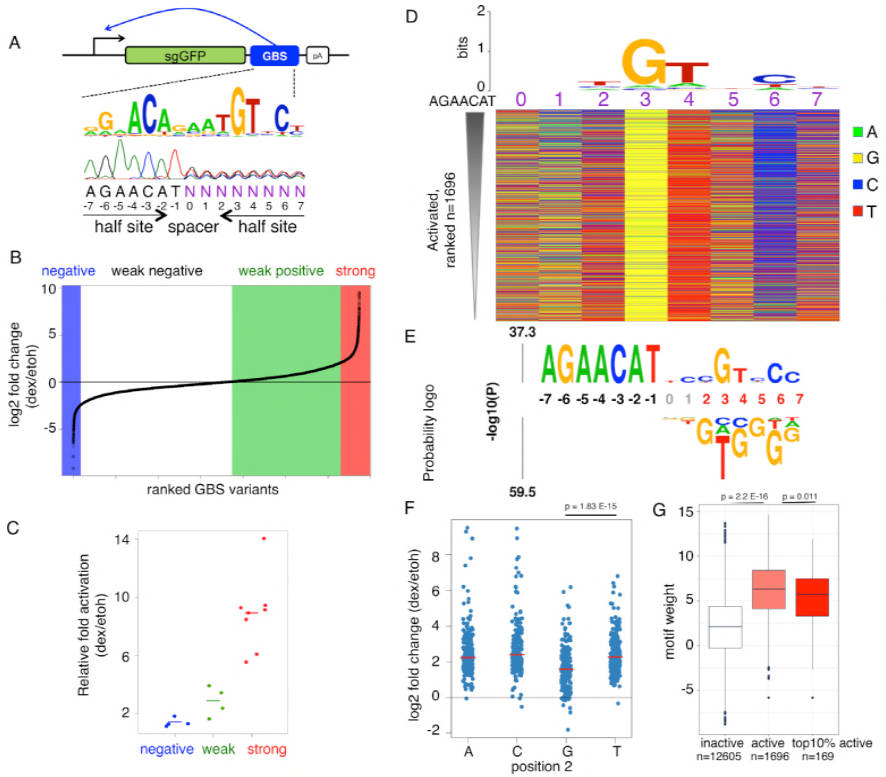

Figure 4. Analysis of the GBS half site library. (a) SynSTARR-seq reporter setup using a synthetic library containing 65536 candidate GR Binding Sequence (GBS) variants (half site library with 8 variable positions N). (b) Candidate GBS variants were ranked by their fold change in expression in response to hormone treatment (4 h, 1 µM dex). Only sequences with a mean read count > 100 across all replicates (n=3) for both dex and ethanol vehicle treated cells are shown. Repressed (log2 FC < -2), weakly active (0 < log2 FC <2) and activated GBS variants (log2 FC ≥ 2) are highlighted by a blue, green and red background respectively. (c) The enhancer activity of negative (n=4), weak (n=4) and strong (n=8) GBS variants was assessed by qPCR for individually transfected STARR-seq constructs. Fold change upon dexamethasone treatment normalized to the activity for the scrambled control plasmid is shown. Horizontal line shows the mean for each activity group; dots the values for individual constructs. (d) Top: Consensus motif and below a color chart summarizing the sequence at each variable position for each significantly activated GBS variant (adjusted p-value < 0.01) ranked by their fold change in response to dex treatment. (e) *k*pLogo probability logo (activity logo) for half site variants depicting the p-values from Mann-Whitney U tests of whether GBS variants with a specific nucleotide at a given position are more (displayed above number indicating nucleotide position) or less (displayed below number indicating nucleotide position) active than other GBS variants. Positions with significant nucleotides ($p < 0.001$) are highlighted in red, fixed positions in black. (f) Log2 fold change upon dexamethasone treatment for GBS-like variants with either an A, C, G or T at position 2 (exact match to AGAACATnnXGTnCn, with X either A,C,G or T). Data for individual sequences are shown as blue dots. Horizontal red lines show the median for each group. p-values were calculated using a Student's t-test. (g) Boxplot of the motif weight (using the truncated 15nt long M00205 motif from Transfac) for inactive (-0.5≤ log2 fold change ≤0.5; white), active (light red) and the top 10% active (dark red) GBS variants. p-values were calculated using a Student's t-test.

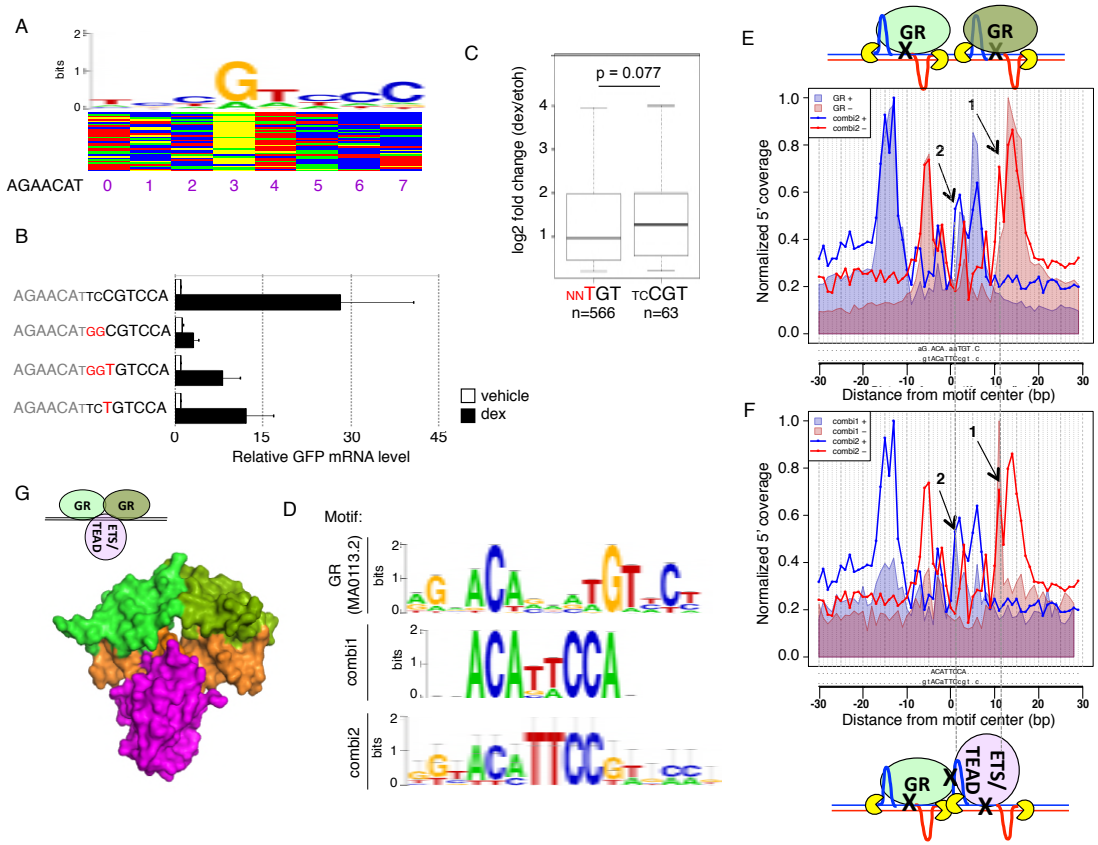

Figure 5. Identification and characterization of the combi2 motif. (a) Color chart for the top activated GBS variants and above the consensus motif for the 25 most active sequences (b) Transcriptional activity of STARR-seq reporters containing candidate GBS variants as indicated. Relative RNA levels ± S.E.M. are shown for cells treated with ethanol vehicle and for cells treated overnight with 1 µM dexamethasone (n = 3). (c) Boxplot of the log2 fold change upon treatment for 4 h with 1 µM dexamethasone for genes with a ChIP-seq peak in the region ±20 kb around the TSS containing either a conventional GBS match (M00205; p value <0.0001) or a combi2-like sequence (combi2 motif; p value < 0.0001). Center lines show the median. p-value was calculated using the Wilcoxon rank sum test. (d) Motif logo representing the positional weight matrices for the canonical GBS (JASPAR MA0113.2), combi1 and combi2 motif. (e) Alignment of the ChIP-exo footprint profiles for the combi2 and the conventional GBS motif. Arrows 1 and 2: Additional 5' coverage for the combi2 motif that does not match the conventional GBS footprint. (f) Alignment of the ChIP-exo footprint profiles for the combi1 and combi2 motif. Arrows 1 and 2: Additional 5' coverage for the combi2 motif when compared to the GBS footprint aligns with signal for the combi1 footprint. (g) Structural alignment of combined binding of a GR dimer (green) and ETS1 (purple, middle: PDB 1K79) at the combi2 sequence (orange).

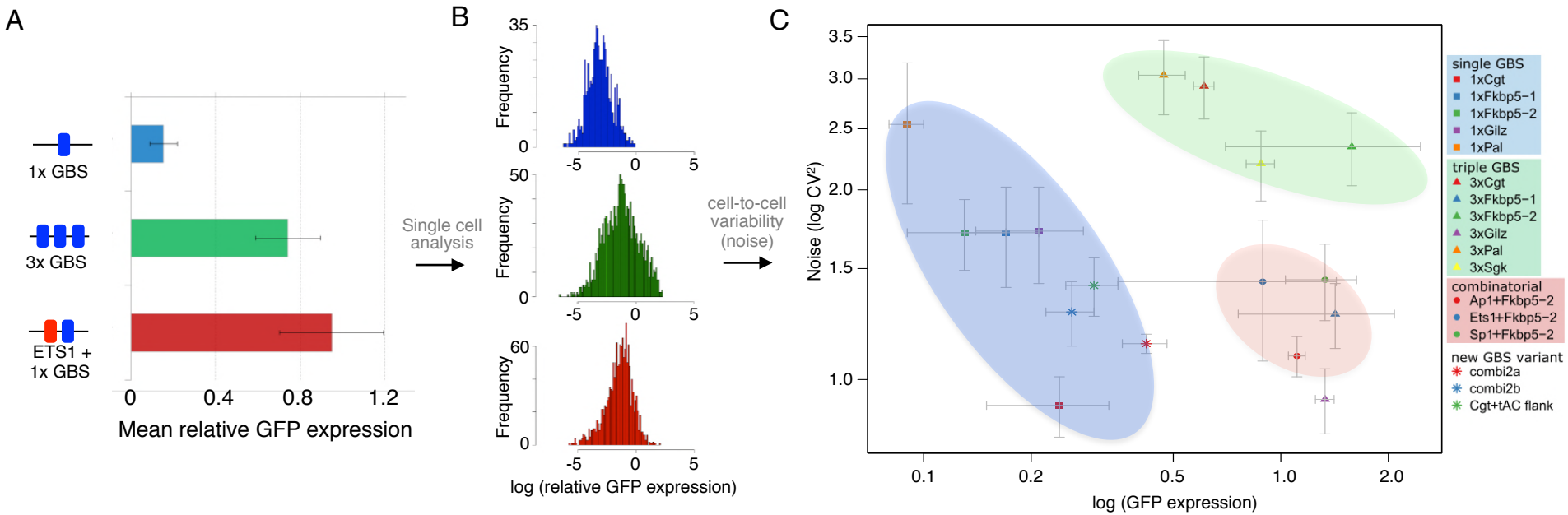

Figure 6. The effect of GBS sequence, number and presence of other TFBS on transcriptional output and noise. (a) Mean GFP expression relative to mCherry of the STARR-seq reporter for cell populations treated overnight with 1 μM dexamethasone with binding site variant as indicated was determined by flow cytometry. (b) The single-cell distribution of GFP expression relative to co-transfected mCherry was determined for each binding site variant as indicated by flow cytometry. The mean and noise for each binding site variant are extracted from these distributions (see Methods). (c) Average and S.D. for mean GFP expression and for noise from three biological replicates. Area with mostly single GBS variants is highlighted with a blue background; Area with three GBSs with a green background and area with composite binding sites consisting of a single GBS and a binding site for another TF with a red background.

Supplementary figures

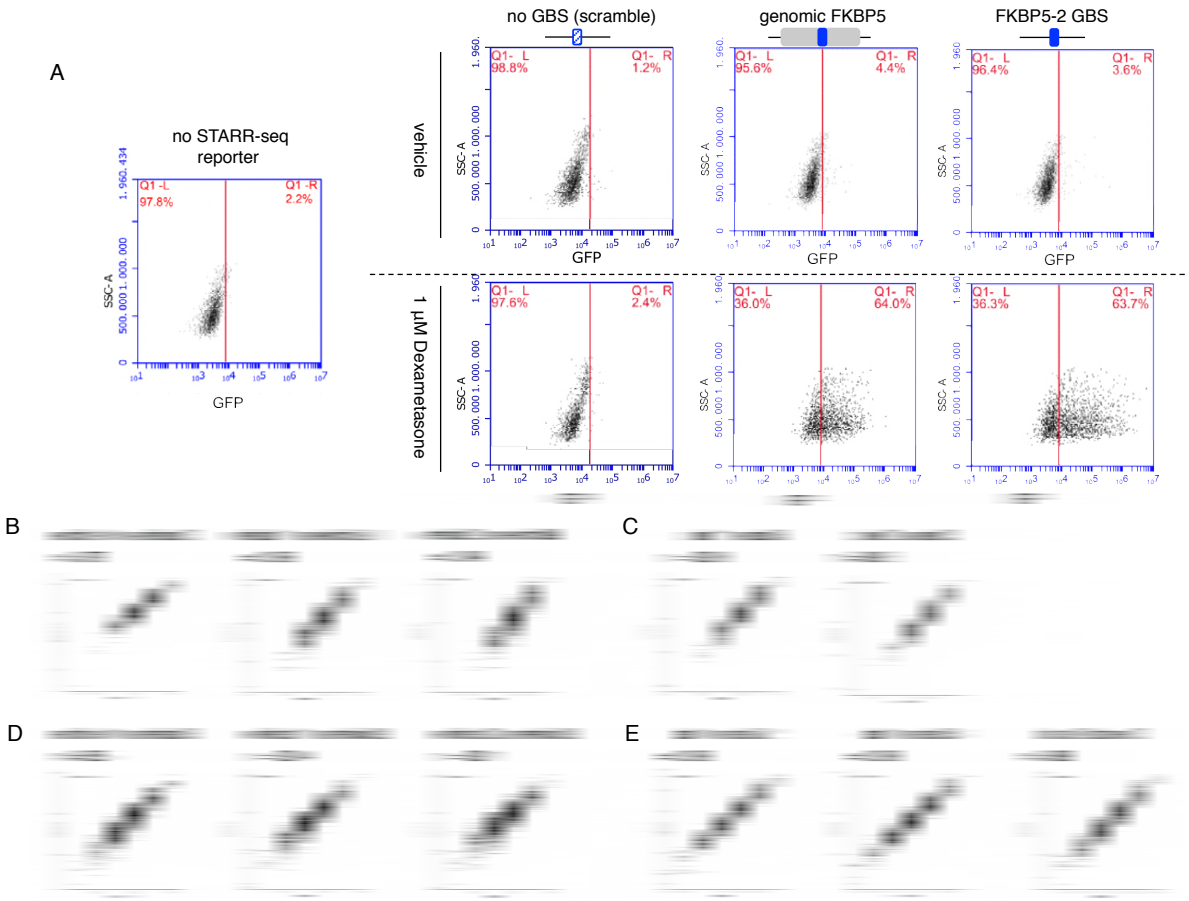

Figure S1. Analysis of individual enhancer variants by flow cytometry and synSTARR-seq reproducibility. (a) Analysis of individual enhancer variants as indicated by flow cytometry showing the side scatter (SSC-A) versus GFP signal for individual mCherry-positive cells. Left: no STARR-seq construct. Right-Top: ethanol, vehicle, treated cells; Right-Bottom: Cells treated overnight with 1µM dexamethasone. Numbers in red indicate the percentage of GFP+ (top right side) and GFP- (top left side) cells respectively. Red vertical line demarcates the threshold for being called GFP+. (b) RNA-seq correlation plots for biological replicates of vehicle-treated cells transfected with the GBS-flank library (Cgt flank library). (c) Same as (b) except for biological replicates of dexamethasone-treated cells (4h 1µM). (d) RNA-seq correlation plots for biological replicates of vehicle-treated cells transfected with the GBS-flank library (Sgk flank library). (e) Same as (d) except for biological replicates of dexamethasone-treated cells (4h 1µM).

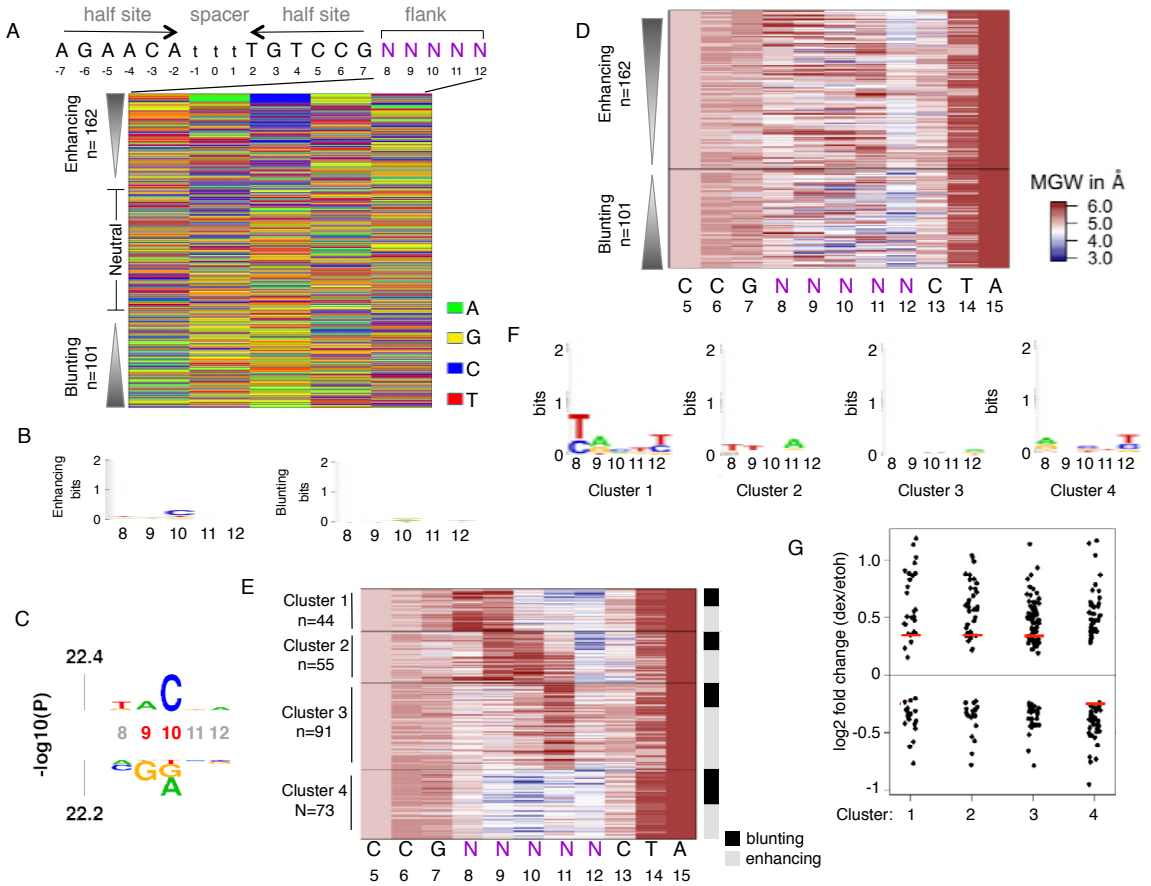

Figure S2. Analysis of the Sgk flank library. (a) Color chart summarizing the sequence at each variable position for flank variants ranked by their fold change in response to hormone treatment. (b) Consensus motif for (left) significantly enhancing and (right) blunting flank variants (c) *k*pLogo probability logo (activity logo) for flank variants depicting the p-values from Mann-Whitney U tests of whether GBS variants with a specific nucleotide at a given position are more (displayed above number indicating nucleotide position) or less (displayed below number indicating nucleotide position) active than other GBS variants. Positions with significant nucleotides ($p < 0.001$) are highlighted (red coordinates). (d) Predicted minor groove width (MGW) for significant enhancing and blunting flank variants of the Sgk GBS library ranked by their fold change in response to hormone treatment. (e) K-means clustering based on MGW for significantly enhancing and blunting flank variants. Right side: activating and blunting variants are highlighted in grey and black respectively. (e) Consensus sequence motif for clusters as indicated. (g) Log2 fold change upon dexamethasone treatment for each cluster as indicated. The synSTARR-seq activity for individual sequences is shown as black dots, the median for each group as a horizontal red line.

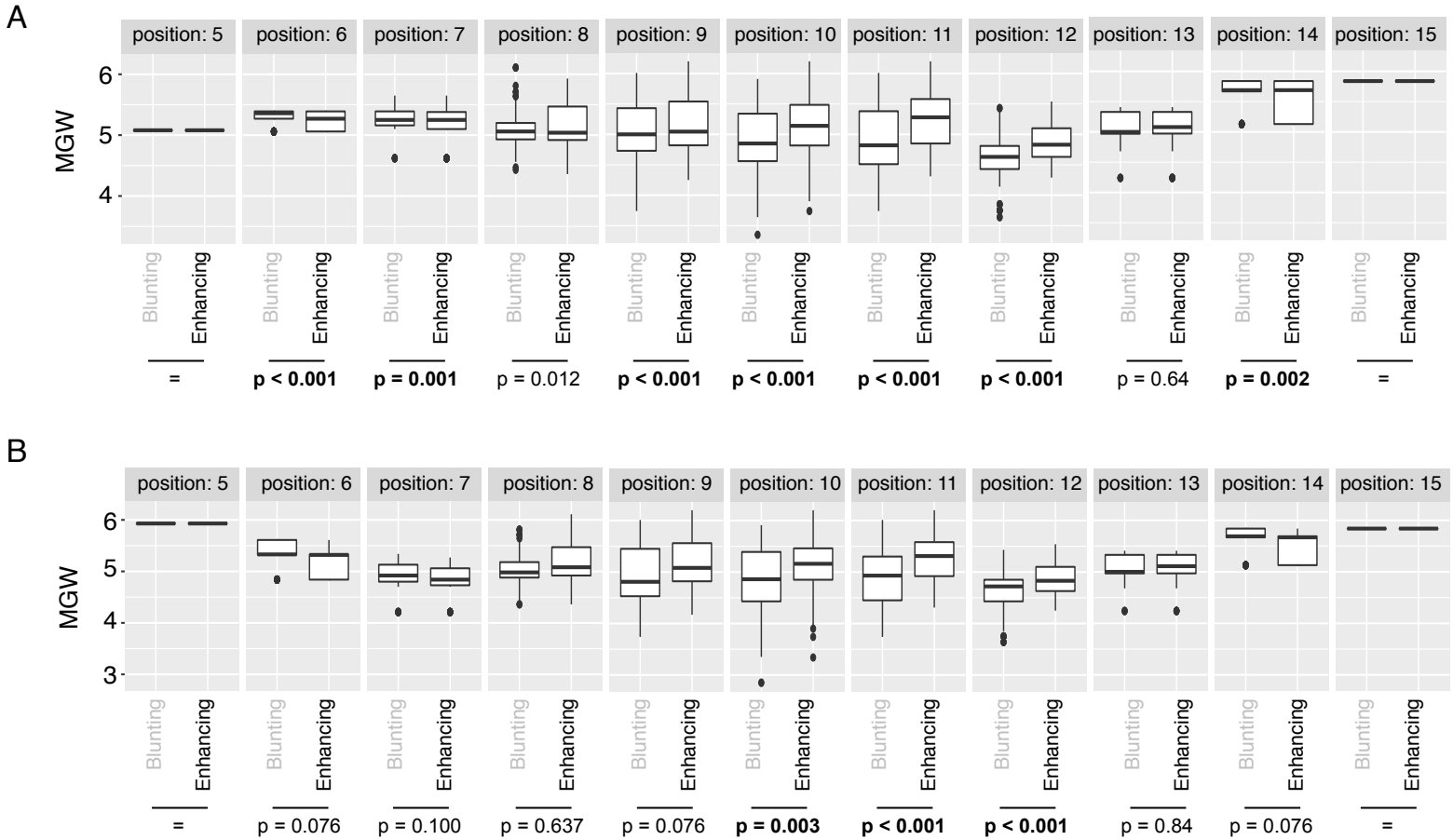

Figure S3. MGW comparison between blunting and enhancing flanks. (a) Minor groove width (MGW) for selected individual bases for significantly blunting (n=189) and significantly enhancing (n=125) flanks for the Cgt library. p-values were calculated using the Wilcoxon rank-sum test. (b) Same as for (a) except for significantly blunting (n=162) and significantly enhancing (n=101) flanks of the Sgk flank library.

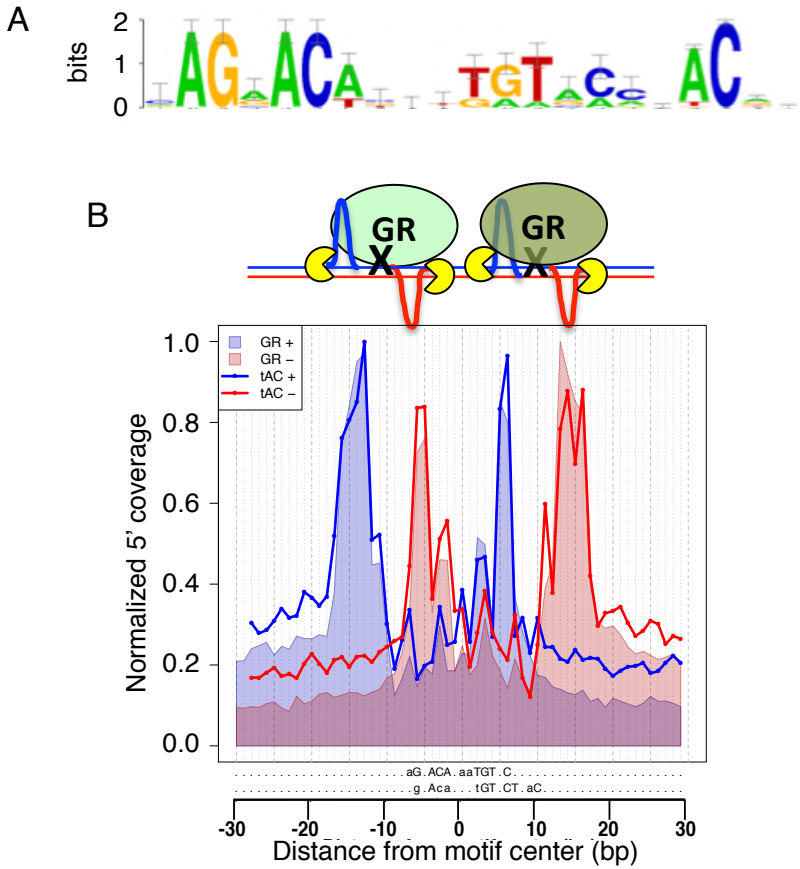

Figure S4. Analysis of the nACnn flank. (a) Motif logo representing the positional weight matrix of highly active flank variants that was used to scan for motif-matches to generate the ChIP-exo footprint profile. (b) Alignment of the ChIP-exo footprint profiles for highly active flank variant matches (p value <0.0001; solid lines: blue: positive strand, red: negative strand) and for the conventional GBS motif (M00205; p value <0.0001; shaded areas; blue: positive strand, red: negative strand).

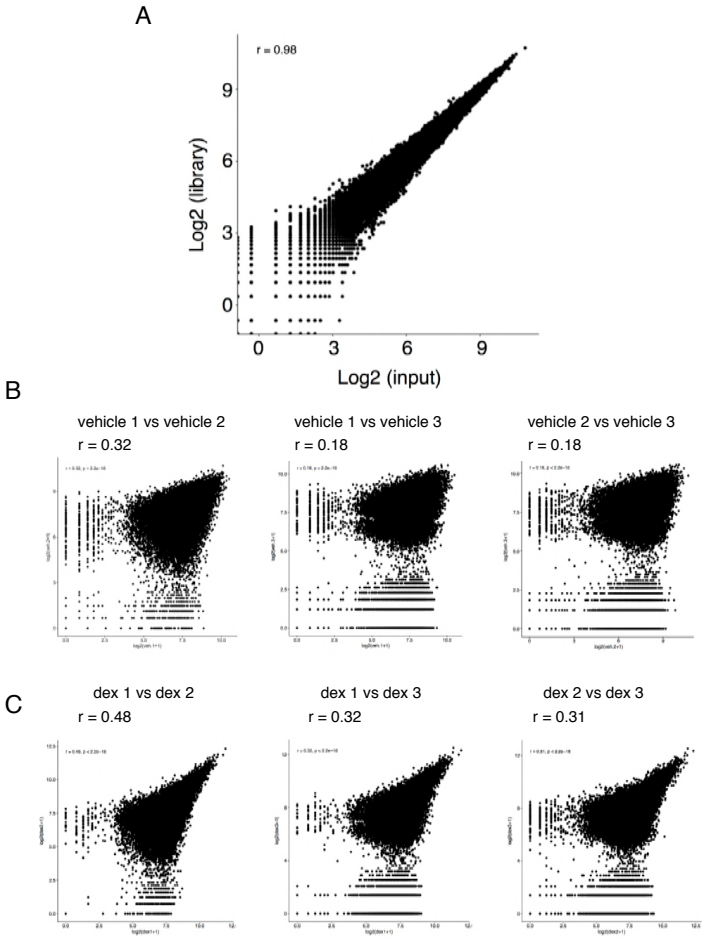

Figure S5. synSTARR-seq reproducibility for the half site library. (a) Correlation plot between input library (library) and the plasmid library isolated from transfected U2OS-GR18 cells (input). (b) RNA-seq correlation plots for biological replicates of vehicle-treated cells. (c) Same as for (b) except for biological replicates of dexamethasone-treated cells (4h 1μM).

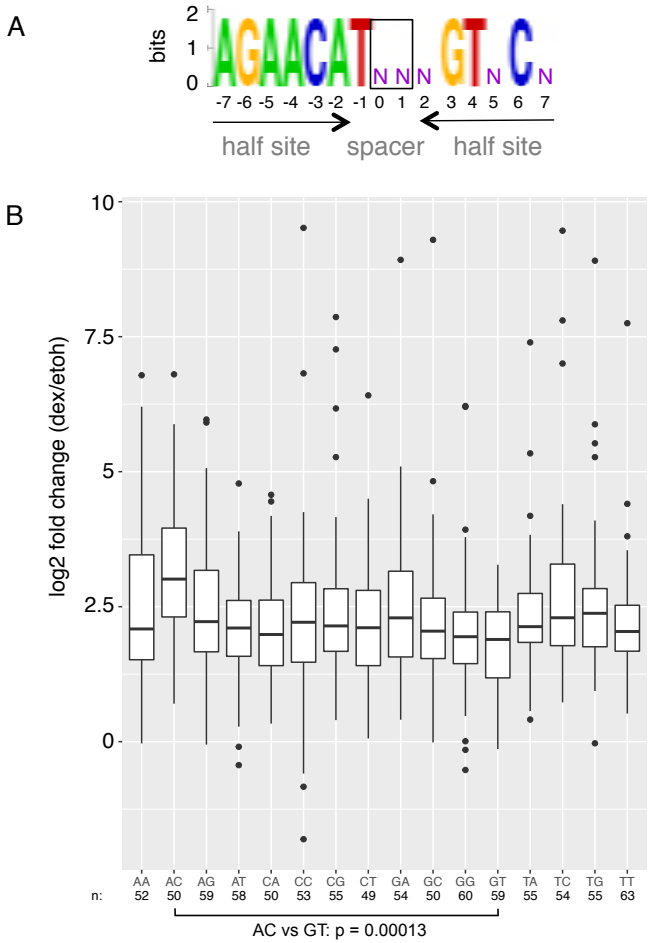

Figure S6. Effect of spacer sequence on GBS activity. (a) Motif logo representing the sequence that was used to scan for GBS-matches in the half site library. Black box highlights the two positions in the spacer whose effect on GBS activity was assayed. (b) Boxplot of the log2 fold change upon treatment for 4 h with 1 μM dexamethasone for GBS matches with spacer variant as indicated. Center lines show the median. The Benjamini-Hochberg corrected p-value for the spacer variants with the most significance difference was calculated using a Student's t-test.

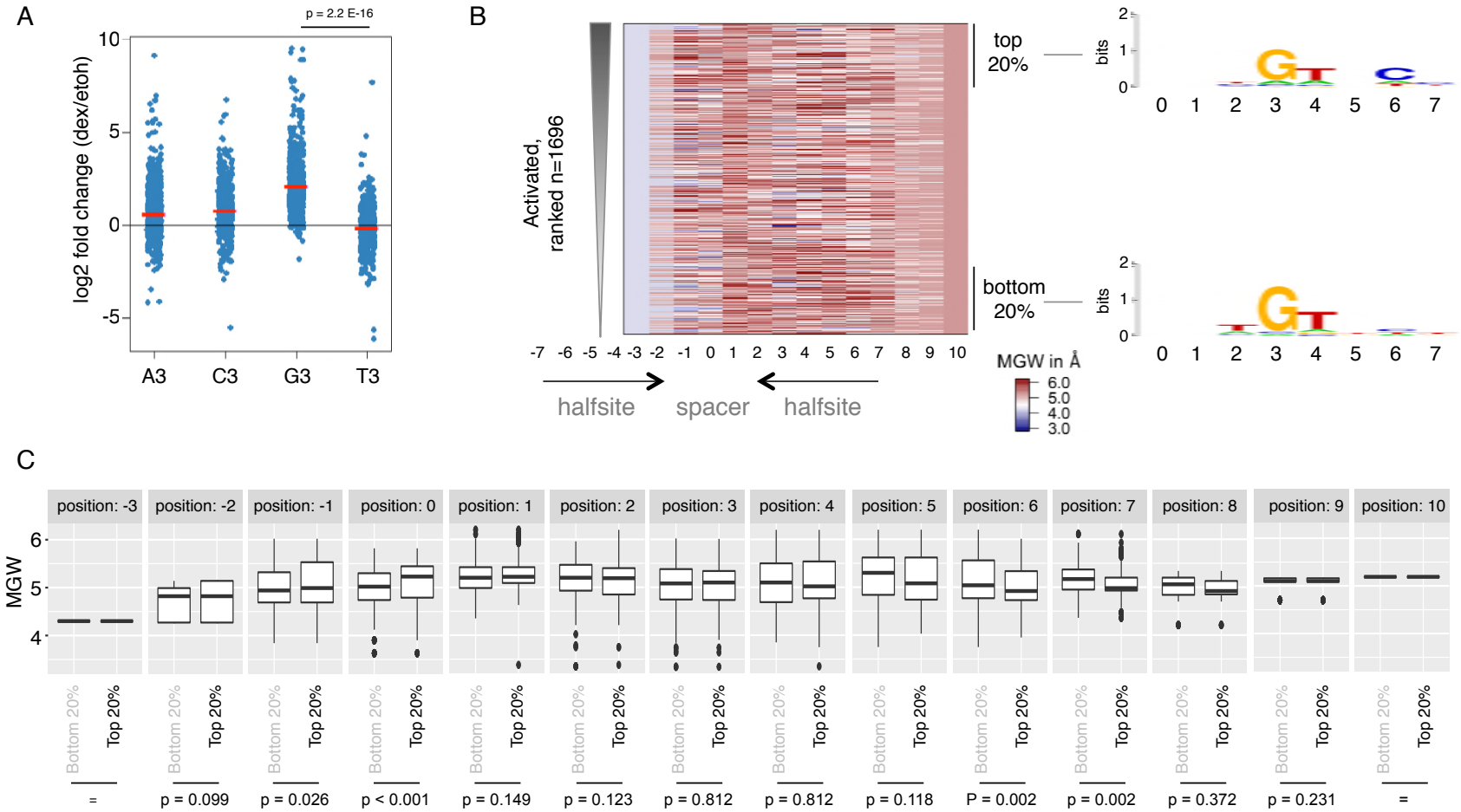

Figure S7. Analysis of the GBS half site library. (a) Log2 fold change upon dexamethasone treatment for active GBS variants with either an A, C, G or T at position 3. Data for individual sequences that match consensus second half site at key positions 4 and 6 (exact match to AGAACATnnnXTnCn, with X either A,C,G or T) are shown as blue dots. Horizontal red lines show the average for each group. p-value was calculated using a Student's t-test. (b) Left: Minor groove width (MGW) prediction for GBS variants ranked by activity. Right: Consensus motif for top 20% most active and bottom 20% least active GBS variants. (c) MGW for select individual bases comparing the top 20% most active and bottom 20% least active activated GBS variants. p-values were calculated using the Wilcoxon rank-sum test.

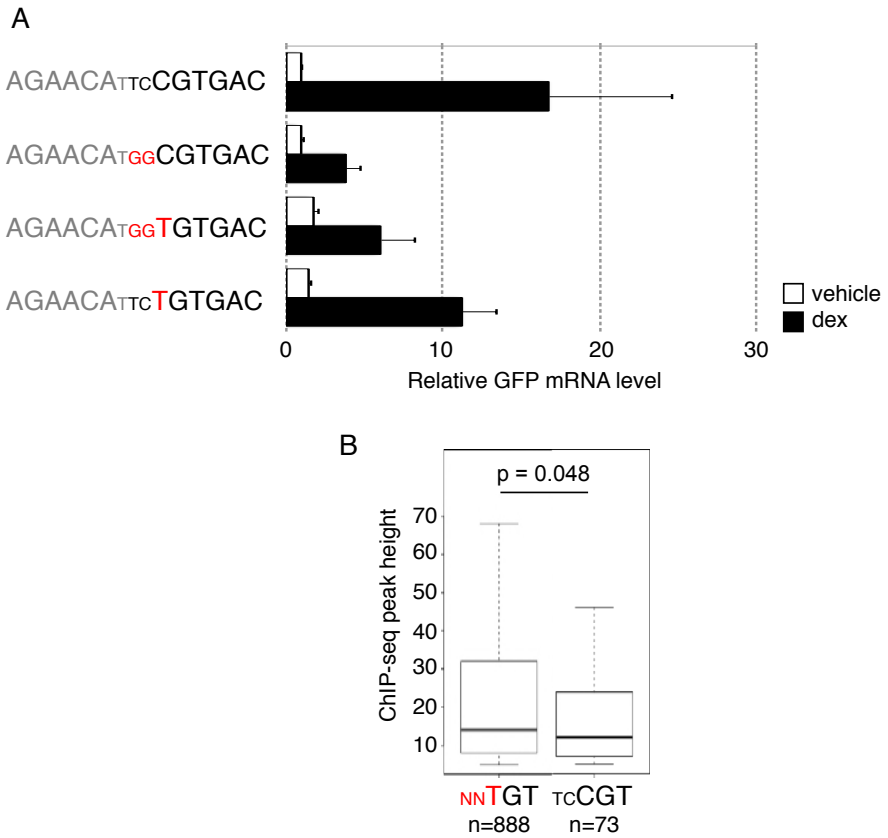

Figure S8. Characterization of the combi2 motif. (a) Transcriptional activity of STARR-seq reporters containing candidate GBS variants as indicated. Relative RNA levels ± S.E.M. are shown for cells treated with ethanol vehicle and for cells treated overnight with 1 μM dexamethasone (n = 3). (b) Boxplot showing the peak-height for GR target genes with either a canonical GBS motif match (nnTGT) or a combi2 motif match (tcCGT). Center lines show the median, p value was calculated using a Wilcoxon rank-sum test.

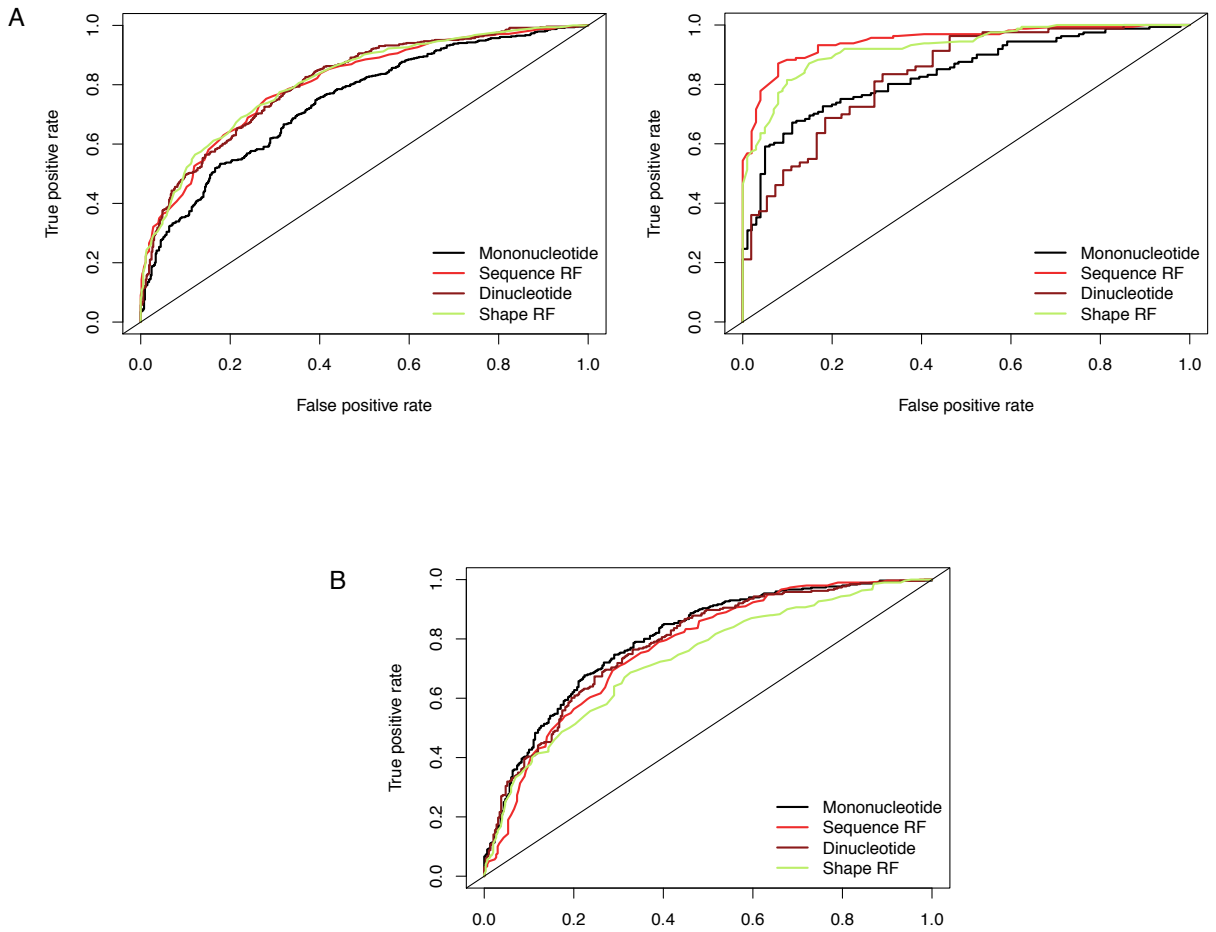

Figure S9. Prediction of GBS activity based on DNA sequence or DNA shape. (a) ROC curves analyzing the ability of the models to distinguish between blunting and enhancing flank variants for (left) the Cgt flank library; (right) the Sgk flank library. Mononucleotide: Classifier based on mononucleotide frequencies within the two classes. Dinucleotide: Classifier constructed using dinucleotide frequencies. Sequence Random Forest (RF): Random Forest classifer trained and tested on coded nucleotide sequences. Shape Random Forest (RF): Random forest classifier based on predicted MGW. (b) Same as for (a) except that model and ROC curves where trained and assessed for their ability to discriminate between the top and bottom 20% significantly active GBS variants from the half site library.